

Anomalous diffusion and directed coalescence of condensates out of equilibrium

Andriy Goychuk^{1, 2, 3}

¹*Institute for Medical Engineering and Science, Massachusetts Institute of Technology, Cambridge, MA 02139, United States*

²*Department of Systems Immunology, Helmholtz-Center for Infection Research, 38124 Braunschweig, Germany*

³*Lower Saxony Center for Artificial Intelligence and Causal Methods in Medicine (CAIMed), Hannover, Germany**

(Dated: October 14, 2025)

Phase separation into domains with distinct composition and properties has widespread implications, ranging from alloys and emulsions to biomolecular condensates in cells. In living and nonliving matter, the organization of these domains can be controlled by nonequilibrium chemical reactions, external fields, or mechanical stresses. In this context, stationary states can emerge from long-range monopolar interactions analogous to electrostatics. More generally, as discussed here, because fluxes induce dipolar force fields, externally controlled boundary motion effectively polarizes the domain even for microscopically nonpolarizable matter. The dipole-dipole interactions resulting from this *translation-induced polarization* cause directed coalescence of domains. This coarsening mechanism complements Ostwald ripening and coalescence due to Brownian motion or Marangoni flows, and has implications for controlling domains by electric fields or concentration gradients. Interestingly, the chemical potential gradients around a domain that nucleates material are exactly opposite to the hydrodynamic pressure gradients around an impermeable colloid that pushes the fluid, suggesting a competition between phase separation and hydrodynamics. In addition to chemical control, the motion of domains can also be driven by mechanical stresses. An example is the cell interior, where mechanical stresses are actively generated by molecular motors and opposed by passive viscoelastic stresses in the cytoplasm and nucleoplasm. The resulting fluid flows lead to Brownian motion with a suppressed or enhanced size scaling which modifies collision-coalescence. For active stresses with a long correlation time, the domains show superdiffusion on intermediate time scales. Together, these findings shed new light on the dynamics of domains in viscoelastic media and conserved order parameters in general.

Phase separation is a recurrent phenomenon in various disciplines. Its mathematical description was originally developed in the context of polymer melts [1–3] and alloys [4, 5], spanning soft matter and materials science, has implications for chemical engineering, including batteries and reactors [6, 7], and has been most recently applied to cell biology. In the cell, phase separation contributes to spatial organization by sorting molecules according to their relative miscibility [8–14]. The resulting biomolecular condensates have been implicated in vital processes such as gene transcription [15–19], splicing [20], and assembly of ribosomal subunits [21, 22].

Phase-separated domains undergo coarsening through various mechanisms, including ripening driven by surface tension [23] and coalescence due to Marangoni flows or Brownian motion [24, 25]. To functionalize phase-separated domains in the context of engineering and biology, their spatial positioning and thermodynamically driven coarsening must be controlled. However, it is not clear how the prescribed motion of one phase-separated domain will affect nearby domains. In the context of rigid colloidal particles embedded in a viscous fluid, this is a well-studied problem [26, 27]. In the context of phase-separated domains, it will be shown that existing theoretical frameworks need to be extended.

In a realistic setting, phase-separated domains are typically embedded in a viscoelastic medium [28]. In the

case of the cell, the functions of many intracellular condensates involve interactions with chromatin [29, 30] or the cytoskeleton [31–33]. This coupling makes condensates sensitive to viscous and elastic stresses and can, for example, mechanically drive ripening or arrest coarsening [34–39]. In contrast to the well-studied dynamics of colloidal particles diffusing in viscoelastic media [40, 41], the dynamics of phase-separated domains are much less explored in this context.

The cell cytoskeleton generates active stresses [42], chromatin undergoes correlated motion [43–45], and the viscoelastic medium in an engineered system can be actively stirred. Active forces are known to accelerate the diffusion of rigid particles [46] and are thus expected to facilitate the coalescence of biomolecular condensates [47]. However, beyond this qualitative expectation, the Brownian motion of phase-separated domains in active viscoelastic media is not well understood. Another important caveat is that stirring can also suppress phase separation [48, 49] as observed in active nematic fluids [50, 51], which will not be further explored here.

The main goal of the present work is to better understand the motion of phase-separated domains in a nonequilibrium setting. To that end, using an exact analytical framework, we will discuss two paradigmatic problems.

First, how do pairs of phase-separated domains interact when they move due to an external potential gradient, such as gravitation, an electrostatic potential, or a concentration gradient? In analogy to viscous fluids and electrostatics, where incompressibility and charge con-

* andriy@goychuk.me

servation lead to nonlocal disturbances and interaction forces [26], phase-separating solutions show similar effects due to mass conservation [52]. Even in media that cannot be polarized microscopically, the motion of phase-separated domains induces chemical potential gradients that are reminiscent of the electrical field around an electrostatic dipole. In the following, this effect will be referred to as *translation-induced polarization*.

The resulting chemical potential gradients are opposite to the pressure gradient generated by colloidal particles moving through a viscous fluid, because phase-separated domains nucleate material through a gain in enthalpy at the phase boundaries, contrary to the mechanics of impermeable domain walls. Nearby phase-separated domains sense these chemical potential gradients and are drawn towards the front of larger domains, thereby driving directed coalescence. This prediction complements the ripening of phase-separated domains under external fields [53, 54] and can be tested experimentally [55, 56].

Second, what are the signatures of the Brownian motion of individual phase-separated domains in actively fluctuating viscoelastic media? This fundamental question has led to the Stokes-Einstein relation [40, 57], which couples fluctuations and dissipation, and which has sparked countless studies in the context of colloidal particles. In the context of phase-separated domains, however, studies considering Brownian motion are more scarce [58–62]. To close this gap, this work reports an ordinary differential equation describing the mean squared displacement of phase-separated domains in fluctuating media with memory.

As a specific application, we discuss how active stress fluctuations in a viscoelastic Maxwell fluid, as an oversimplified model for the cell cytoplasm and nucleoplasm, can modify the Brownian motion of condensates. Compared with the Stokes-Einstein relation, active stresses can suppress or amplify the scaling of condensate motion of domain size, thereby altering the kinetics of coalescence.

DROPLET MOTION INDUCES DIPOLE FORCES

In the following, phase-separated domains are indicated as regions with locally increased concentration $c(\mathbf{x}, t)$ of, for example, proteins or nucleic acids. The dynamics of these molecules can generally be categorized into mass-conserving material fluxes, with mobility M , and material turnover on some time scale k^{-1} . Phase separation is a consequence of fluxes that redistribute mass along the gradients in the chemical potential, μ , which encodes an internal trade-off between entropy and enthalpy, until the system has settled in thermodynamic equilibrium [63, 64].

To enable external control, one can apply the potential Ψ . This could correspond to, for example, an electrostatic or gravitational field or molecular interactions when there is a gradient in the concentration of another

molecule. Importantly, it can also absorb stochastic forces if one allows Ψ to fluctuate. For generality and because we will later discuss advection by fluid flow, I will also consider fluxes \mathbf{j} that cannot be written as the streamlines of some potential.

For material turnover, I will consider exchange with an external reservoir maintained at constant chemical potential μ^* and separated by a transition state corresponding to some chemical potential barrier $\bar{\mu}$. Taking Arrhenius kinetics for chemical reactions, which is thermodynamically consistent [65, 66], leads to a degradation rate $ke^{-\beta(\bar{\mu}-\mu)}$ and a recovery rate $ke^{-\beta(\bar{\mu}-\mu^*)}$ with the standard notation $\beta = 1/(k_B T)$. In summary, the dynamics of the concentration profile $c(\mathbf{x}, t)$ is given by

$$\begin{aligned} \partial_t c = \nabla \cdot [M \nabla \mu + M \nabla \Psi - \mathbf{j}] \\ + ke^{-\beta(\bar{\mu}-\mu^*)} - ke^{-\beta(\bar{\mu}-\mu)}. \end{aligned} \quad (1)$$

This general formalism can also be applied beyond the dynamics of condensates to conserved Ising models, or active matter, to name a few examples. Following Ref. [67] which studied condensate self-propulsion in the absence of hydrodynamics semianalytically, Eq. (1) will in the following be interpreted as a control problem and, therefore, the chemical potential as unknown. Thus, all subsequent results are independent of microscopic details.

It is well known that the chemical potential in phase separation problems satisfies a Poisson equation and thus mediates nonlocal interactions resembling electrostatics as discussed, for example, in Ref. [52]. This was also used as the basis of a recent preprint [68] on the motion and deformations of droplets under thermophoresis, which I became aware of after making an earlier version of this work available [69]. In the following, I will use these non-local interactions to predict how pairs of droplets should interact under external gradients and contrast this to the hydrodynamic interactions between colloids in viscous fluids.

From the perspective of electrostatics, Eq. (1) is analogous to the nonlinear version of the Debye-Hückel theory [70]. For small β , or chemical reactions with small potential barriers, one can use a linear approximation,

$$\nabla \cdot [M \nabla \mu] - k\beta\mu = \partial_t c + \nabla \cdot [\mathbf{j} - M \nabla \Psi] - k\beta\mu^*, \quad (2)$$

where we have collected all terms involving the chemical potential on the left-hand side. The characteristic screening length is given by $\sqrt{M/(k\beta)}$ and, since $M = k_B T/\zeta = 1/(\zeta\beta)$ with microscopic friction coefficient ζ , diverges as $\beta^{-1}(\zeta k)^{-1/2}$ in the limit of high temperature, or small friction, or slow chemical kinetics. Therefore, the following analysis will focus on the unscreened limit.

To build intuition for the resulting chemical potential gradients, consider a prescribed perturbation of the concentration, $\partial_t c(\mathbf{x}, t) := \delta c(\mathbf{x})\delta(t)$. Because mass exchange enters as a source or sink in the Poisson equation,

Eq. (2), a local production or degradation of material is analogous to an electric monopole inducing an electrostatic potential [66, 71]. For a moving phase boundary, mass is removed from one side and added to the opposing side of the interface, resembling a local electric dipole with source $\partial_t c(\mathbf{x}, t) = -\nabla \cdot [\mathbf{v}(t)c(\mathbf{x}, t)]$. This suggests that translation will induce dipole force fields, whereas shape changes will lead to higher-order multipole fields, even in matter that is not polarizable microscopically.

To make a comparison to colloidal particles in a viscous fluid, the following analysis will consider phase-separated domains with spherical shape and radius R . This is a decent approximation for high surface tension, but neglects multipole interactions due to capillary waves. Assuming stable condensates, their domains \mathcal{D} will change mainly due to translation and rotation and will therefore be approximately conserved. The role of the chemical potential is to maintain phase separation with a high concentration $c(\mathbf{x}, t) = c_- + \Delta c$ inside the condensate, $\mathbf{x} \in \mathcal{D}$, and a low concentration $c(\mathbf{x}, t) = c_-$ outside. In that sense, the chemical potential can be interpreted as a Lagrange multiplier that enforces the conservation of the shape of the condensate boundary during translation, similar to how the pressure field guarantees incompressibility in fluids. From this analogy to fluid mechanics, it is not surprising that perturbations in the condensate interface propagate non-locally and induce long-range forces.

In agreement with the above reasoning, moving the condensate with velocity $\mathbf{v}(t) = \partial_t \mathbf{r}(t)$ induces an effective long-range force (Fig. 1A, Appendix A)

$$-\nabla \mu(\mathbf{x}, t) = \nabla \Psi(\mathbf{x}, t) - \frac{\Delta c}{M} \mathcal{B}(\mathbf{x} - \mathbf{r}) \cdot \mathbf{v}(t) + \mathcal{O}[\mathbf{j}], \quad (3)$$

where $\mathcal{B}(\mathbf{z}) = R^d [\hat{\mathbf{z}} \otimes \hat{\mathbf{z}} - \mathbf{I}/d]/|\mathbf{z}|^d$ for large distances $|\mathbf{z}| \gg R$ is the Green's tensor for a dipole field and $\mathcal{O}[\mathbf{j}]$ is a functional of order \mathbf{j} . In summary, the motion of phase-separated domains, regardless of the underlying driving force, universally induces dipole force fields. In the following, I refer to this phenomenon *translation-induced polarization* as opposed to motion that arises from pre-existing polarity.

Equation (3) also reveals an important difference compared to the dynamics of colloids in viscous fluids. Because phase-separated domain walls nucleate material, whereas impermeable walls push the fluid, the chemical potential gradient is exactly opposite to the pressure gradient generated by a moving solid particle (Fig. 1B). This competition will be analyzed in more detail in future work on the interactions between pairs of phase-separated domains. For now, I will focus on the consequences of the dipole-like chemical potential gradients.

DROPLET MOTION IN RESPONSE TO FORCES

So far, we have discussed how the motion of one phase-separated domain will induce chemical potential (and potentially also hydrodynamic pressure) gradients. Now,

we will recapitulate how these forces will cause other phase-separated domains to move in response. For simplicity, I will consider the limit of negligible material turnover, $k \rightarrow 0$. Independently of other microscopic details, the velocity of a droplet governed by Eq. (2) is then given by [67, 72]

$$\mathbf{v}(t) = \partial_t \mathbf{r}(t) = -\frac{d}{\Delta c} \int_{\mathcal{D}(t)} \frac{d^d \mathbf{x}}{V_{\mathcal{D}}} M \nabla \Psi(\mathbf{x}, t) - \frac{d}{\Delta c} \int \frac{d^d \mathbf{x}}{V_{\mathcal{D}}} \mathcal{B}(\mathbf{x}) \cdot \mathbf{j}(\mathbf{x}, t). \quad (4)$$

where $V_{\mathcal{D}}$ is the volume and $\mathcal{D}(t)$ the time-dependent domain of the phase-separated droplet centered around $\mathbf{r}(t)$. This *force-response relation* follows directly by applying the thermodynamic consistency criterion [67]

$$\int_{\mathcal{D}(t)} d^d \mathbf{x} \nabla \mu(\mathbf{x}) = 0, \quad (5)$$

which can also be interpreted as the conservation of momentum for the droplet (Appendix A), to the chemical potential gradient, Eq. (3). By combining the quantification of droplet motion in response to local force fields, Eq. (4), with the understanding of how droplet motion generates dipole forces, Eq. (3), I will next analyze pairwise interactions between droplets in a dynamic, nonequilibrium setting.

PAIRS OF MOVING DROPLETS INTERACT LIKE DIPOLES

The results so far revealed that the material fluxes around self-propelling condensates, which were reported in Ref. [67] for density-dependent mobility, are a manifestation of the dipole force field [Eq. (3), Fig. 1A]. As a consequence of these fluxes and following the discussion so far, it is natural to expect pairs of moving condensates to show dipole-dipole interactions according to an effective polarization along their direction of motion. These interactions emerge due to the conservation of the total mass of the phase-separating material, while the dipole and quadrupole interactions seen in active matter are mediated by the surrounding medium [74–77].

For self-propelling magnetic dipoles in external flow, long-range interactions can lead to clustering [78]. The theory predicts a similar effect for droplets in external flow due to their emergent dipolar interactions. Specifically, inducing condensate motion with velocity \mathbf{v} (for example, by sedimentation or phoresis) will cause two phase-separated domains of different sizes R_1 and R_2 to move relative to each other according to (Fig. 1C)

$$\partial_t (\mathbf{r}_2 - \mathbf{r}_1) \approx (R_2^3 - R_1^3) \nabla \otimes \nabla \frac{1}{|\mathbf{r}_2 - \mathbf{r}_1|} \cdot \mathbf{v}, \quad (6)$$

where \mathbf{r}_1 and \mathbf{r}_2 are the centers of mass. The smaller condensate will be drawn towards the leading side of

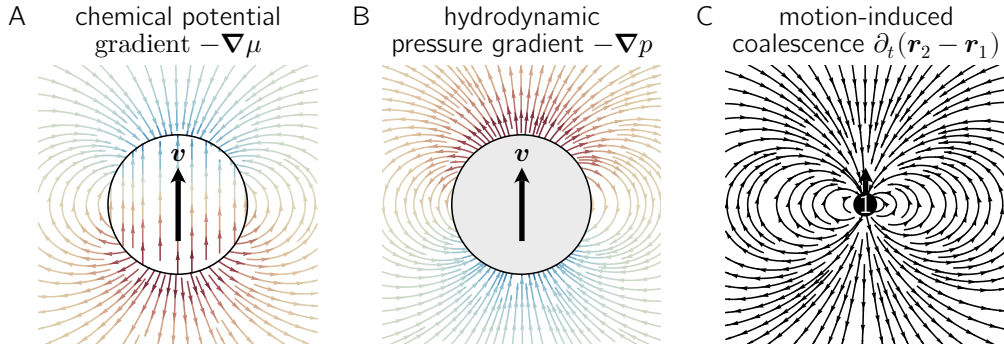


FIG. 1. Emergent phenomena induced by translational motion (velocity \mathbf{v} , black arrow) of biomolecular condensates and in domain-forming systems in general. A) Translational motion of domains of conserved order parameters (outlined by black line) induces long-ranged forces that are reminiscent of electrostatic dipoles (stream lines). Streamlines indicate the gradient of the chemical potential (color code; red corresponds to high values and blue to low values). B) Impermeable boundaries push fluid when they move. Therefore, the pressure gradients around moving colloidal particles in a Stokes fluid [73] are opposite to the chemical potential gradients around moving droplets. This suggests a competition between phase separation and fluid flow. Streamlines indicate the gradient of the pressure (color code; red corresponds to high values and blue to low values). C) Translational motion leads to directed coalescence, where smaller condensates circle around and flow (black stream lines) towards the leading edge of larger condensates (black circle with label “1”). If hydrodynamic interactions dominate, smaller condensates may circle towards the trailing edge of a larger condensates.

the larger condensate, so that even passive condensates undergo directed coalescence under external potential gradients. If hydrodynamic interactions dominate, the flow direction might be reversed, and the smaller droplet could be drawn toward the trailing side of the larger droplet, which will be analyzed in future work. This prediction can be tested in experiments on condensates in external chemical gradients [55], and is consistent with the observation that diffusiophoresis of biomolecules promotes phase separation [56].

How fast is directed coalescence? Assuming self-similarity for the size distribution of the phase-separated domains, the flow velocity is independent of the average condensate size $\langle R \rangle$. With the typical distance between condensates $\propto \langle R \rangle$, this induces collisions with the rate $\propto \langle R \rangle^{-1}$, so that the average condensate size will increase over time as $\langle R \rangle \propto t$. This result is analogous to how hydrodynamic interactions and surface tension can cooperate to increase coalescence rates during the late stages of phase separation [24]. In contrast, for coalescence by Brownian motion, the diffusion coefficient scales as $\propto R^{-1}$ and, over distances $\propto \langle R \rangle$, induces collisions with the rate $\propto \langle R \rangle^{-3}$, leading to the usual $\langle R \rangle \propto t^{1/3}$ scaling. Thus, intuitively, it is expected that directed coalescence will dominate over long time scales.

Beyond applying external fields to control the dynamics, condensate motion can also emerge as a consequence of chemical reactions. Such chemical reactions can lead to effective (screened) monopole interactions [22, 71, 79], whereas the motion of condensates leads to dipole interactions, and capillary waves correspond to multipole couplings. By combining these mechanisms, I hypothesize that chemically active, self-propelling condensates [80, 81] can form stable flocks. These ideas can find potential application to mass-conserved reaction-

diffusion systems if one can map them to a generalized Cahn-Hilliard model [82]. This has potentially far-reaching consequences for understanding the formation of dynamical patterns in reaction-diffusion systems.

BROWNIAN MOTION OF CONDENSATES

So far, we have discussed how pairs of phase-separated domains will deterministically interact with each other under an external field. This includes, for example, sedimentation due to gravitation, or phoresis in an electric field with parallel field lines. On large length scales, the phase-separated domains resemble pointlike objects with positions $\mathbf{r}(t)$. Agitations by passive and active fluctuating forces drive the stochastic Brownian motion of these objects, with random velocities $\mathbf{v}(t) = \partial_t \mathbf{r}(t)$, which is well characterized for colloidal particles. In the following, I will analyze the Brownian motion of droplets in a viscoelastic solvent driven by passive and active fluctuations, with a view toward describing condensates in the cell cytoplasm or nucleoplasm.

Condensates in random fluid flows

The force-response relation, Eq. (4), characterizes the motion of phase-separated domains due to potential and nonpotential currents. The stochastic motion of the constituent particles can be modeled, in the inviscid limit, by applying a fluctuating potential Ψ that drives random thermal currents $\mathbf{j}_{th} := -M \nabla \Psi$ with zero mean and covariance $\langle \mathbf{j}_{th}(\mathbf{x}, t) \otimes \mathbf{j}_{th}(\mathbf{x}', t') \rangle = 2Mk_B T \mathbf{I} \delta(\mathbf{x} - \mathbf{x}') \delta(t - t')$. This is sometimes referred to as *Model B* [83]. On sufficiently large length scales, one also needs to take

into account advection by stochastic hydrodynamics with flow velocity \mathbf{v}_f . The resulting nonpotential fluxes enter through $\mathbf{j} := c \mathbf{v}_f$, which cannot be cast as a gradient. In summary, the velocity of the condensate is given by

$$\mathbf{v} = \frac{d}{\Delta c} \int_{\mathcal{D}(t)} \frac{d^d \mathbf{x}}{V_{\mathcal{D}}} \mathbf{j}_{th}(\mathbf{x}, t) + \int_{\mathcal{D}(t)} \frac{d^d \mathbf{x}}{V_{\mathcal{D}}} \mathbf{v}_f(\mathbf{x}, t). \quad (7)$$

The main focus of the present manuscript is on the second term in Eq. (7), which intuitively states that the condensate is advected by the average flow.

The subsequent analysis will, for simplicity, neglect the feedback of condensate motion on the hydrodynamics. On sufficiently large length scales and far away from physical boundaries, fluid flows induced by the long-range chemical potential gradient [Eq. (3)] will resemble those generated by a point force (Appendix C). These fluid flows are of the order $\mathcal{O}(\Delta c^2)$ and decay as $1/M$ for large mobilities M (Appendix C). However, this also raises the fundamental question of how one can measure the chemical potential gradients induced by condensate motion. Moreover, long-range chemical potential gradients [Eq. (3)] induced by the random motion of condensates will directly lead to Casimir-like forces. This is an interesting topic for future research because of the aforementioned competition between hydrodynamics and phase separation.

For further simplicity, I will assume that the fluctuating hydrodynamic flows \mathbf{v}_f and the thermal currents \mathbf{j}_{th} induced by microscopic collisions are independent random variables. The resulting Brownian motion of the condensate is characterized by the velocity autocorrelation function

$$\begin{aligned} \frac{1}{2} \partial_t^2 \text{MSD}(t - t') &= \langle \mathbf{v}(t) \cdot \mathbf{v}(t') \rangle = D_c \delta(t - t') \\ &+ \iint_{\mathcal{D}} \frac{d^d \mathbf{z}}{V_{\mathcal{D}}} \frac{d^d \mathbf{z}'}{V_{\mathcal{D}}} \langle \mathbf{v}_f(\mathbf{r} + \mathbf{z}, t) \cdot \mathbf{v}_f(\mathbf{r}' + \mathbf{z}', t') \rangle, \end{aligned} \quad (8)$$

where $\text{MSD}(t - t') := \langle |\mathbf{r}(t) - \mathbf{r}(t')|^2 \rangle$ is the mean squared displacement and $D_c := 2d^3 M k_B T / (\Delta c^2 V_{\mathcal{D}})$ is an effective macroscopic diffusion coefficient. Here and in the following, the shorthand notation $\mathbf{r} \equiv \mathbf{r}(t)$ and $\mathbf{r}' \equiv \mathbf{r}(t')$ will refer to the time-dependent displacement of the condensate. Note that terms lacking temporal correlations could here be simplified using $\mathbf{r}(t) \sim \mathbf{r}(t')$ because they are nonzero only for $t = t'$. In contrast, the second line of Eq. (8) requires a more careful analysis because temporal correlations can effectively quench the flow landscape navigated by the phase-separated domains.

Random flows at random locations

The difficulty in analyzing Eq. (8) is that not only the fluid flow but also the droplet center $\mathbf{r}(t)$ around which this flow is observed are time-dependent random variables. To better understand the consequences of this

geometric coupling, we consider a series expansion of the fluid flow velocity field around the midpoint $\bar{\mathbf{r}} := (\mathbf{r} + \mathbf{r}')/2$ of the condensate trajectory. The full series expansion in Appendix D, together with the approximation that hydrodynamic fluctuations are much faster than condensate Brownian motion, shows the following:

$$\begin{aligned} &\langle \mathbf{v}_f(\mathbf{r} + \mathbf{z}, t) \cdot \mathbf{v}_f(\mathbf{r}' + \mathbf{z}', t') \rangle \\ &\approx \exp \left[\frac{1}{2d} \langle [\mathbf{r} - \mathbf{r}']^2 \rangle \nabla_{\mathbf{z}}^2 \right] \mathcal{C}_f(\mathbf{z} - \mathbf{z}', t - t'), \end{aligned} \quad (9)$$

where $\mathcal{C}_f(\mathbf{z} - \mathbf{z}', t - t') := \langle \mathbf{v}_f(\mathbf{z}, t) \cdot \mathbf{v}_f(\mathbf{z}', t') \rangle$ quantifies the hydrodynamic fluctuations. In essence, this result describes how the stochastic motion of the condensate effectively smears out the observed correlations in the fluid flow. This approximation will be used in the following to study fluid flows with finite correlation times.

Dynamics of the condensate center

Instead of the velocity autocorrelation function, it is more convenient to track the mean squared displacement of the phase-separated domain. The memory effects arising from the interplay between condensate motion and hydrodynamic fluctuations, Eq. (8) and Eq. (9), lead to the following second-order differential equation (Appendix E):

$$\frac{1}{2} \partial_t^2 \text{MSD}(t) = \left\langle \exp \left[\frac{\text{MSD}(t)}{2d} \nabla^2 \right] \mathcal{C}_f(\mathbf{z} - \mathbf{z}', t) \right\rangle_{\mathcal{D}}, \quad (10)$$

defined for $t > 0$, where $\langle \dots \rangle_{\mathcal{D}}$ indicates spatial averaging over the coordinates \mathbf{z} and \mathbf{z}' inside the phase-separated domain \mathcal{D} . This can be solved numerically, for spherical condensates with radius R , by using the Fourier transform $\hat{\mathcal{C}}_f(|\mathbf{q}|, \omega) := \int d^d \mathbf{z} \int dt e^{-i\mathbf{q} \cdot \mathbf{z} - i\omega t} \mathcal{C}_f(|\mathbf{z}|, t)$ of the hydrodynamic fluctuations. The initial conditions are given by $\text{MSD}(0) = 0$ and $\partial_t \text{MSD}(0^+) = D_0$, where

$$D_0 = D_c + \frac{d \Gamma(1 + \frac{d}{2})}{\pi^{d/2} R^d} \int_0^\infty \frac{dq}{q} J_{d/2}^2(qR) \hat{\mathcal{C}}_f(q, \infty), \quad (11)$$

characterizes the fluctuations of the condensate center of mass on short time scales due to temporally independent kicks. Here, the Bessel function of the first kind, $J_{d/2}$, accounts for the geometry of the condensate.

To better understand the memory encoded in Eq. (10), we will briefly discuss the dynamics on time scales shorter than the correlation time of the fluid. To that end, I will consider advection in a quenched landscape characterized by $\hat{\mathcal{C}}_f(q, \omega) = q^n \delta(\omega)$. In this case, Eq. (10) is equivalent to $\partial_t^2 \text{MSD} \sim \text{MSD}^{-(d+n)/2}$ for $n > -d$ which leads to $\text{MSD} \sim t^{4/(2+d+n)}$ after a scaling ansatz. In $d = 3$ dimensions, this corresponds to superdiffusion with exponent $4/3$ for quenched hydrodynamic flows ($n = -2$, Fig. S1A), or subdiffusion with exponent $4/5$ for motion in a quenched random potential landscape ($n = 0$).

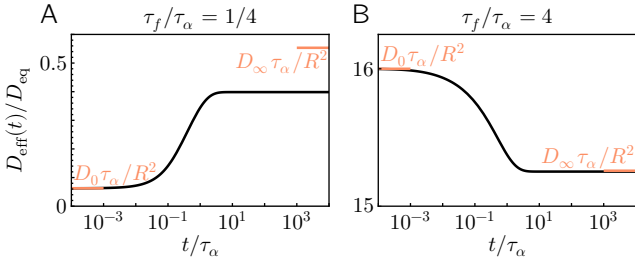


FIG. 2. Effective diffusion coefficient $D_{\text{eff}}(t) := \partial_t \text{MSD}(t)$ of a condensate in a viscoelastic medium compared to Brownian motion $D_{\text{eq}} := 6k_B T/(5\pi\eta R)$ in thermal equilibrium. A) For $\tau_\alpha > \tau_f > 0$, condensate motion is suppressed. Smaller values of τ_f/τ_α further reduce the growth rate of $\text{MSD}(t)$ and hence the decay of $\exp[-q^2 \text{MSD}(t)/6]$ in Eq. (10). This affects the fidelity of the asymptotic limits [Eq. (11) and Eq. (12), red lines] compared to the numerical solution of Eq. (10) [solid lines]. B) For $\tau_\alpha < \tau_f$, condensate motion is enhanced relative to thermal equilibrium. For the parameters chosen here, the diffusivity depends only weakly on the time scale. In both panels, the Fourier number, which relates the stirring time to the characteristic time of diffusive mass transport, is $\text{Fo} = D_{\text{eq}}\tau_\alpha/R^2 = 100$ and hydrodynamic screening is assumed to be negligible $\gamma \approx 0$.

Hence, phase-separated domains can show anomalous diffusion on short to intermediate time scales; please refer to Ref. [84] for an in-depth discussion of anomalous diffusion.

On long time scales, the motion of the condensate is characterized by the effective diffusion coefficient (Appendix F)

$$D_\infty = D_c + \int_{-\infty}^{\infty} dt \left\langle \exp\left[\frac{\text{MSD}(t)}{2d} \nabla^2\right] \mathcal{C}_f(\mathbf{z} - \mathbf{z}', t) \right\rangle_D, \quad (12)$$

where we make the approximation that the smearing out of the observed fluid flow is dominated by condensate motion on very short time scales, $\text{MSD}(t) \approx D_0 |t|$. The dynamics on long time scales can be either faster, or actually slower than the motion on very short time scales determined by D_0 .

The intuition for the theoretical framework discussed so far is as follows. Without temporal correlations in the fluid flow, the motion of the condensate from coordinate $\mathbf{r}(t)$ to $\mathbf{r}(t')$ is accompanied by a complete loss of information about the flow landscape. In that case, the dynamics of the condensate motion will resemble an equilibrium system, with diffusion coefficient $D_0 = D_\infty$ given by Eq. (11). In contrast, in the case of a persistent fluid flow landscape, the condensate has a memory of its past trajectory. This memory can either amplify the motion of the condensate by “surfing” along the most likely currents or suppress transport by “trapping” the condensate. In summary, the theory describes how the memory introduced by active forces, for example, due to cytoskeletal stirring, will affect the dynamics of condensates.

Condensates in an active Maxwell fluid

The theory discussed so far is agnostic to the material properties of the condensate and the solvent. I will now apply this framework to study a specific model system that couples phase separation with fluctuating hydrodynamics [59, 62, 73, 85, 86]. To this end, we will start by discussing the hydrodynamic fluctuations, encoded in the correlation function \mathcal{C}_f , for an incompressible viscoelastic fluid with hydrodynamic screening borrowed from the Brinkman model [87]. For unsteady flow at low Reynolds numbers, the corresponding balance of forces reads

$$\rho \partial_t \mathbf{v}_f = \nabla \cdot \boldsymbol{\sigma} - \nabla p - \eta \gamma \mathbf{v}_f + [\nabla \cdot \boldsymbol{\alpha} - c \nabla \mu], \quad (13)$$

where ρ is the density of the fluid. The pressure p enforces incompressibility, $\nabla \cdot \mathbf{v}_f = 0$, similar to how the chemical potential μ enforces droplet cohesion in Eq. (2).

Viscoelastic effects are incorporated through the Maxwell model, $\tau_f \partial_t \boldsymbol{\sigma} + \boldsymbol{\sigma} = \eta [\nabla \otimes \mathbf{v}_f + (\nabla \otimes \mathbf{v}_f)^T]$, with viscosity η and elastic relaxation time τ_f . The term in square brackets in Eq. (13) can be identified as an applied force field, which maps to the resulting fluid flows via the following Fourier-transformed Green’s function,

$$\hat{\mathcal{G}}(\mathbf{q}, \omega) = \frac{1}{\eta} \left[\frac{q^2}{1 + i\tau_f \omega} + \gamma + i\omega \frac{\rho}{\eta} \right]^{-1} \left[\mathbf{I} - \frac{\mathbf{q} \otimes \mathbf{q}}{q^2} \right]. \quad (14)$$

Although the present manuscript considers the specific choice of a Maxwell fluid, in general one can use the same framework to study other complex fluids or even solids such as the Kelvin-Voigt model. In the following, for simplicity, the discussion is based on an approximation for steady flows, $\omega\rho/\eta \approx 0$, which precludes studying the effect of Basset forces.

These fluid flows are driven by the random stress tensor $\boldsymbol{\alpha}$ which can have passive and active parts. To interpolate between thermal-like and active stresses in the steady-flow approximation $\omega\rho/\eta \approx 0$, I will consider a random stress tensor with exponential memory,

$$\langle \alpha_{ij}(\mathbf{x}, t) \alpha_{kl}(\mathbf{x}', t') \rangle = \frac{k_B T \eta}{\tau_\alpha} e^{-\frac{|t-t'|}{\tau_\alpha}} \delta(\mathbf{x} - \mathbf{x}') \times \left[\delta_{ik} \delta_{jl} + \delta_{il} \delta_{jk} - \frac{2}{d} \delta_{ij} \delta_{kl} \right]. \quad (15)$$

In the limit of vanishing stress correlation time (also referred to as stirring time), $\tau_\alpha \rightarrow 0$, this converges to the fluctuating hydrodynamic stresses expected in a Stokes fluid [88], which has vanishing relaxation time $\tau_f \rightarrow 0$. From the perspective of the generalized Langevin equation, the scenario $\tau_\alpha = \tau_f$ satisfies the fluctuation-dissipation theorem [89] and therefore corresponds to thermal equilibrium. The ratio between these time scales provides a handle on tuning the nonequilibrium dynamics of the viscoelastic fluid and the embedded condensate.

As discussed previously, condensates do not significantly affect the fluid flow if the mobility M is large or the

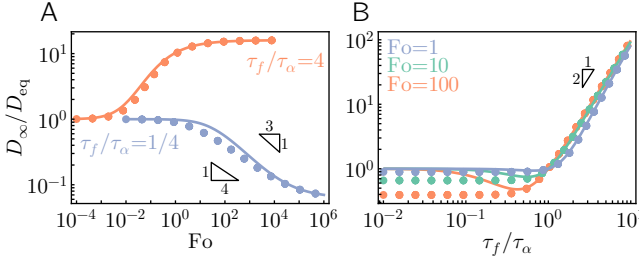


FIG. 3. Diffusion coefficient of condensates on long time scales, relative to thermal equilibrium ($\tau_f = \tau_\alpha$), as a function of A) the Fourier number $Fo := 6k_B T \tau_\alpha / (5\pi\eta R^3)$ and B) the ratio between the fluid relaxation time τ_f and the stress correlation time τ_α . Solid lines represent analytical approximations, dots represent numerical calculations. For simplicity, hydrodynamic screening is assumed negligible, $\gamma \approx 0$.

concentration jump Δc at the droplet boundary is small. Relaxing this approximation (Appendix C) would allow us to calculate fluctuation-induced interactions between condensates, which is reserved for future work. The linear response [Eq. (14)] to the active stress fluctuations [Eq. (15)] predicts that the velocity fluctuations in the viscoelastic fluid are characterized by

$$\frac{\eta \hat{\mathcal{C}}_f(\mathbf{q}, \omega)}{k_B T} = \frac{2(d-1)q^2}{(q^2 + \gamma)^2 + \gamma^2 \tau_f^2 \omega^2} \frac{1 + \tau_f^2 \omega^2}{1 + \tau_\alpha^2 \omega^2}. \quad (16)$$

Note that for spatially uncorrelated *active forces* with exponential memory, as opposed to *active stresses* [Eq. (15)], this expression would be modified by dividing by q^2 . In this case, the growth rate of the mean squared displacement according to Eq. (10) would diverge as $\propto \gamma^{-2+d/2}$ on short time scales. Physically, this implies that in $d < 4$ dimensions and in the absence of hydrodynamic screening, spherical condensates are always unstable with respect to active forces, leading to condensate splitting or shape fluctuations.

Active stirring can enhance or suppress motion

To make concrete predictions, I will now further specialize the theory to spherical condensates with radius R in $d = 3$ dimensions. Moreover, I will study a simplified scenario in which the screening length is large compared to the condensate size, $\sqrt{\gamma}R \ll 1$, on sufficiently long time scales so that $\gamma R^2 \tau_f / t \ll 1$. With these approximations, the flow correlations of the viscoelastic fluid [Eq. (16)] can be simplified to

$$\frac{\eta \hat{\mathcal{C}}_f(\mathbf{q}, \omega)}{k_B T} \approx \frac{4q^2}{q^4 + 2\gamma q^2} \frac{1 + \tau_f^2 \omega^2}{1 + \tau_\alpha^2 \omega^2}. \quad (17)$$

For $\tau_\alpha = \tau_f$, which satisfies the fluctuation-dissipation theorem, the last term in Eq. (17) vanishes. Hence, the Brownian motion of condensates on long time scales can

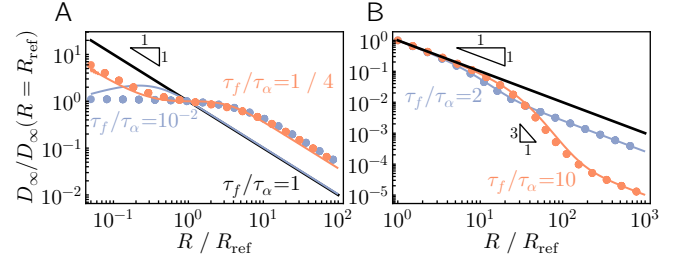


FIG. 4. Effective diffusion coefficient of a condensate with radius R , compared to a reference condensate with radius R_{ref} . Solid lines indicate analytical approximations, while dots represent numerical calculations, where $Fo = 1000$ for the reference radius R_{ref} . A) For $\tau_f < \tau_\alpha$, there is a crossover regime where the diffusion coefficient is largely independent of condensate radius. Note that the analytical approximation fails when $\tau_f \ll \tau_\alpha$. B) For $\tau_f > \tau_\alpha$, there is a crossover regime where the diffusion coefficient departs from the Stokes-Einstein scaling. The width of this crossover regime increases with τ_f/τ_α . For simplicity, hydrodynamic screening is assumed negligible, $\gamma \approx 0$.

only differ from the fluctuations on short time scales, $D_0 \neq D_\infty$, if $\tau_\alpha \neq \tau_f$.

Figure 2 shows the slope of the mean squared displacement for two scenarios, $\tau_\alpha < \tau_f$ and $\tau_\alpha > \tau_f$. On short time scales, the mean squared displacement of the condensate grows with the effective diffusion coefficient [Eq. (11)]

$$D_0 \approx D_c + \frac{6k_B T}{5\pi\eta R} \frac{\tau_f^2}{\tau_\alpha^2} \left[1 - \frac{5\sqrt{\gamma}R}{3\sqrt{2}} \right], \quad (18)$$

to lowest order in $\sqrt{\gamma}R$. For small condensates, $R < 35$ nm estimated in Appendix G, motion is dominated by $D_c \propto 1/R^3$, and is independent of fluctuations in the viscoelastic fluid. Since one can assume that biomolecular condensates exceed this threshold size in practice, the following discussion will be based on the approximation $D_c \approx 0$. For large condensates, taking into account fluid stresses recovers the size dependence of the Stokes-Einstein relation, $D_0 \propto 1/R$, in agreement with recent Cahn-Hilliard-Navier-Stokes simulations [62]. Compared to a solid object, the hydrodynamic radius of liquid biomolecular condensates is reduced by the factor 5/36. Importantly, shorter stress correlation times τ_α , or longer fluid relaxation times τ_f , amplify the Brownian motion of condensates relative to thermal equilibrium ($\tau_\alpha = \tau_f$).

Next, we will discuss the fluctuations of the center of mass of the condensate on long time scales [Eq. (12)], to lowest order in $\sqrt{\gamma}R$. For large condensates, $R \gg \sqrt{D_0 \tau_\alpha}$, one approximately has

$$D_\infty \approx D_0 + \frac{6k_B T}{5\pi\eta R} \left[1 - \frac{\tau_f^2}{\tau_\alpha^2} \right] \left[1 - \frac{5\sqrt{\gamma}R}{3\sqrt{2}} \right]. \quad (19)$$

Substituting Eq. (18) into Eq. (19) eliminates the dependence on τ_f/τ_α , thus suggesting that large condensates

sates show thermal-like dynamics on long time scales. Together with the previous results, this indicates that condensate motion on long time scales (D_∞) is faster than condensate motion on short time scales (D_0) for longer stress correlation times τ_α or shorter fluid relaxation times τ_f (Fig. 2A). Conversely, condensate motion on long time scales (D_∞) is slower than on short time scales (D_0) for $\tau_f > \tau_\alpha$ (Fig. 2B and Fig. S1B). These analytical predictions are also corroborated by Fig. 3, which directly compares the numerical results with analytical approximations.

Interestingly, the scaling of the effective diffusion coefficient with condensate size changes qualitatively for sufficiently small condensates, $R \ll \sqrt{D_0 \tau_\alpha}$. The analytical approximation,

$$D_\infty \approx D_0 + \frac{\sqrt{6}k_B T}{\pi \eta \sqrt{D_0 \tau_\alpha}} \left[1 - \frac{\tau_f^2}{\tau_\alpha^2} \right] \left[1 - \sqrt{\frac{\gamma D_0 \tau_\alpha}{3}} \right], \quad (20)$$

suggests a potential nonmonotonicity as a function of D_0 and thus condensate radius if $\tau_\alpha > \tau_f$. The numerical calculations clarify that, instead of nonmonotonicity, there is a wide range of condensate sizes where the diffusion coefficient on long time scales, D_∞ , is actually insensitive to the condensate radius (Fig. 4A). Hence, active stirring of the viscoelastic medium has a qualitative effect on the Brownian motion of condensates with potentially far-reaching implications for coalescence. These findings complement the prediction of directed coalescence as a result of motion-induced dipole interactions, which was discussed in the first part of this manuscript.

How will active stirring affect the growth of the condensate radii via collision-coalescence? Turning the effective diffusion coefficient D_∞ independent of condensate size, due to active fluctuations with $\tau_\alpha > \tau_f$ (Fig. 5), increases the scaling exponent $\langle R \rangle \sim t^{1/2}$ of the average condensate radius as a function of time. Once the condensates are sufficiently large, the effective diffusion coefficient recovers the Stokes-Einstein size dependence $D_\infty \propto 1/R$ so that further growth follows the standard $\langle R \rangle \sim t^{1/3}$ law. In contrast, for $\tau_\alpha < \tau_f$, the effective diffusion coefficient scales as $D_\infty \propto 1/R^n$, with $n > 1$, over a wide range of condensate sizes (Fig. 4B, Fig. 5), leading to a reduced scaling exponent $\langle R \rangle \sim t^{1/(2+n)}$. Integrating these findings with the previous results suggests that the rate of coalescence will initially be higher for $\tau_\alpha < \tau_f$ due to a larger effective diffusion coefficient D_∞ and consequently a higher rate of collisions (Fig. 3B). With increasing condensate radii, Brownian motion will be rapidly suppressed (Fig. 4B), thereby creating a bottleneck and skewing the droplet size distribution.

These arguments neglect the fact that moving condensates show dipole-dipole interactions, which should further accelerate coalescence and would be interesting to study in more detail. One simple hypothesis is that hydrodynamic interactions, which couple the motion of condensates over large distances, resemble the motion due to an externally applied field studied in the first part of the

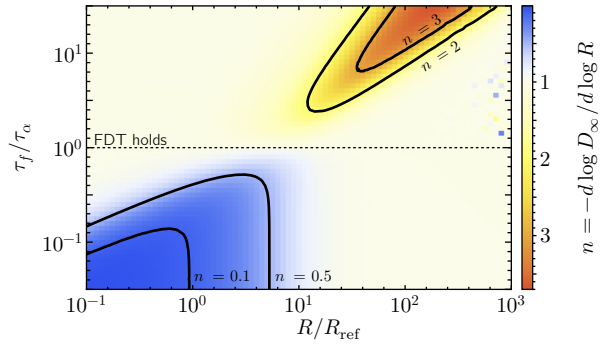


FIG. 5. Scaling of the effective diffusion coefficient with condensate radius, $D_\infty \sim 1/R^n$, compared to a reference condensate with radius R_{ref} and corresponding Fourier number $\text{Fo} = 1000$. In the blue region of the phase diagram, condensate motion is almost independent of condensate size. In the red region of the phase diagram, the dependence of Brownian motion on condensate size is amplified. In all other regions (bright yellow), the Stokes-Einstein relation $D_\infty \sim 1/R$ is recovered. Dashed line corresponds to a passive system where the fluctuation-dissipation theorem (FDT) holds.

manuscript. Based on this reasoning, one would expect to recover the accelerated coalescence $\langle R \rangle \propto t$, which is consistent with studies on the late stages of phase separation [24].

DISCUSSION

In summary, this manuscript presents a framework for studying the Brownian motion of biomolecular condensates in actively driven viscoelastic media. Active stress fluctuations are introduced *ad hoc* by breaking the fluctuation-dissipation theorem. In doing so, one discovers that condensate motion can be either enhanced or suppressed depending on the ratio between the viscoelastic relaxation time τ_f and the correlation time τ_α of the active stress. Moreover, the theory predicts how condensate motion can be decoupled from condensate size, thereby lifting a fundamental limitation on the frequency of collisions in polydisperse solutions. This could potentially find applications in the development of droplet-based chemical reactors, where frequent collisions could lead to the synchronization of reactions via exchange of reactants. Future research will explore this possibility by taking into account enzymatic chemistry.

It would also be interesting to compare the predictions of the analytical theory with existing experiments. For example, recent work has shown that cytoskeletal activity quantitatively increases the frequency of collisions between biologically relevant condensates in the cell nucleus, such as speckles which are involved in RNA splicing [47]. This effect was shown to accelerate coalescence of condensates and affect the chemical reactions within them [47]. To interrogate this system further, one could tune the correlation time τ_α of the active stress fluctu-

ations by changing the residence time of myosin motors on actin filaments, or the relaxation time τ_f of the viscoelastic fluid by tuning the turnover of actin or actin crosslinkers. In addition, tracking the mean squared displacement and size distribution of condensates over time would yield complementary information that would allow inference of model parameters. This would allow testing whether cells typically operate in the $\tau_\alpha > \tau_f$ or in the $\tau_\alpha < \tau_f$ regime and open new avenues for controlling intracellular organization.

Finally, we have discussed that the motion of domain boundaries between conserved phases with different compositions and physical properties will generically induce long-ranged forces reminiscent of electrical dipole fields. This is a universal consequence of mass conservation and therefore applies not just to droplets, but to any conserved domain-forming system. Future research is needed to confirm the predicted phenomenon of directed coalescence, to quantitatively measure the underlying forces, and to understand how the emerging droplet-droplet interactions are affected by viscoelastic stress propagation and impermeable walls.

ACKNOWLEDGMENTS

The author thanks Yannick Azhri Din Omar, Saeed Mahdisoltani, Mehran Kardar, and Arup K. Chakraborty for insightful discussions and critical reading of the manuscript. The author also thanks Eric R. Dufresne for pointing out the possibility of directed coalescence in experiment. This work was supported by the National Science Foundation through the Biophysics of Nuclear Condensates grant (MCB-2044895). During his time at MIT, A.G. was supported by an EMBO Postdoctoral Fellowship (ALTF 259-2022). Part of this work was carried out at HZI with support by the Ministry of Science and Culture of Lower Saxony through funds from the program zukunft.niedersachsen of the Volkswagen Foundation for the ‘CAIMed – Lower Saxony Center for Artificial Intelligence and Causal Methods in Medicine’ project.

SUMMARY DESCRIPTION OF THE APPENDICES

The following appendices provide the technical background and step-by-step calculations for the results reported in the main text.

Appendix A: Derivation of force-velocity relation

This supporting section outlines the derivation of the chemical potential profile μ that controls the dynamics $\partial_t c$ according to Eq. (2). In the following, $\nabla \equiv \nabla_z$ refers to the spatial gradient and \mathcal{D} without time dependence

indicates the condensate domain in the comoving and corotating frame.

To study condensates moving with velocity \mathbf{v} , it is natural to use a traveling wave ansatz, $c(\mathbf{x}, t) = c(\mathbf{z})$ with the coordinate transformation $\mathbf{z} := \mathbf{x} - \mathbf{v}t$. Note that Eq. (2) is a Poisson equation for the chemical potential [52], which leads to:

$$\mu(\mathbf{z}) = -\Psi(\mathbf{z}) + \frac{\Delta c}{M} \mathbf{v} \cdot \int_{\mathcal{D}} d^d z' \nabla \mathcal{L}(\mathbf{z} - \mathbf{z}') - \frac{1}{M} \int d^d z' \mathbf{j}(\mathbf{z}') \cdot \nabla \mathcal{L}(\mathbf{z} - \mathbf{z}'), \quad (\text{A1})$$

with $\mathcal{L}(\mathbf{z})$ the fundamental solution to the Poisson equation $\nabla^2 \mathcal{L}(\mathbf{z}) = -\delta(\mathbf{z})$. The gradient of the chemical potential in the co-moving and co-rotating frame is given by

$$\nabla \mu(\mathbf{z}) = -\nabla \Psi(\mathbf{z}) + \frac{\Delta c}{M} \mathcal{B}(\mathbf{z}) \cdot \mathbf{v} - \frac{1}{M} \int d^d z' [\nabla \otimes \nabla \mathcal{L}(\mathbf{z} - \mathbf{z}')] \cdot \mathbf{j}(\mathbf{z}'), \quad (\text{A2})$$

where the coupling tensor \mathcal{B} is defined by

$$\mathcal{B}(\mathbf{z}) \equiv \mathcal{B}(\mathbf{z}|\mathcal{D}) := \nabla \otimes \nabla \int_{\mathcal{D}} d^d z' \mathcal{L}(\mathbf{z} - \mathbf{z}'). \quad (\text{A3})$$

For spherical condensates with radius R , the above integral can be evaluated:

$$\mathcal{B}(\mathbf{z}) = - \begin{cases} \frac{\mathbf{I}}{d}, & |\mathbf{z}| \leq R, \\ \left[\frac{\mathbf{I}}{d} - \hat{\mathbf{z}} \otimes \hat{\mathbf{z}} \right] (|\mathbf{z}|/R)^{-d}, & |\mathbf{z}| > R. \end{cases} \quad (\text{A4})$$

In essence, this is identical to the Green’s tensor for a dipolar electrostatic field. Transforming Eq. (A2) into the laboratory frame, with shorthand notation $\mathbf{r} \equiv \mathbf{r}(t)$ for the position of the condensate moving with velocity $\mathbf{v} = \partial_t \mathbf{r}$, leads to Eq. (3) reported in the main text.

Using the thermodynamic consistency criterion [67],

$$\int_{\mathcal{D}} d^d z \nabla \mu(\mathbf{z}) = 0, \quad (\text{A5})$$

where \mathcal{D} is the condensate domain in the co-moving and co-rotating frame, the chemical potential can be eliminated:

$$0 = - \int_{\mathcal{D}} d^d z M \nabla \Psi(\mathbf{z}) + \Delta c \int_{\mathcal{D}} d^d z \mathcal{B}(\mathbf{z}) \cdot \mathbf{v} - \int d^d z \mathcal{B}(\mathbf{z}) \cdot \mathbf{j}(\mathbf{z}), \quad (\text{A6})$$

The next step is to substitute Eq. (A4). Note that the result for $\mathbf{z} \in \mathcal{D}$ can also be derived for general geometries by using isotropy, which implies $\mathcal{B} = \text{tr}(\mathcal{B}) \mathbf{I}/d$. Hence, without loss of generality, one has

$$\frac{\Delta c V_{\mathcal{D}}}{d} \mathbf{v} = - \int_{\mathcal{D}} d^d z M \nabla \Psi(\mathbf{z}) - \int d^d z \mathcal{B}(\mathbf{z}) \cdot \mathbf{j}(\mathbf{z}). \quad (\text{A7})$$

where $V_{\mathcal{D}} := \int_{\mathcal{D}} d^d z$ is the condensate volume. The main insight here is that, in contrast to gradient flow dynamics, currents that cannot be represented by the gradient of a potential generically lead to nonlocal couplings.

After substituting random thermal currents for the potential flux, $\mathbf{j}_{th} := -M \nabla \Psi$, and advection through the fluid for the nonpotential flux, $\mathbf{j} := c \mathbf{v}_f$, one has:

$$\frac{\Delta c V_{\mathcal{D}}}{d} \mathbf{v} = \int_{\mathcal{D}} d^d z \mathbf{j}_{th}(z) - \int d^d z c(z) \mathcal{B}(z) \cdot \mathbf{v}_f(z). \quad (\text{A8})$$

Using $c(\mathbf{x}, t) = c_- + \Delta c$ for $\mathbf{x} \in \mathcal{D}$, else c_- , to split the domain integral, leads to:

$$\begin{aligned} \frac{\Delta c V_{\mathcal{D}}}{d} \mathbf{v} &= \int_{\mathcal{D}} d^d z \mathbf{j}_{th}(z) - \Delta c \int_{\mathcal{D}} d^d z \mathcal{B}(z) \cdot \mathbf{v}_f(z) \\ &\quad - c_- \int d^d z \mathcal{B}(z) \cdot \mathbf{v}_f(z), \end{aligned} \quad (\text{A9})$$

The first line can be simplified using Eq. (A4). The second line can be eliminated via integration by parts and invoking fluid incompressibility, $\nabla \cdot \mathbf{v}_f = 0$:

$$\mathbf{v} = \frac{d}{\Delta c} \int_{\mathcal{D}} \frac{d^d z}{V_{\mathcal{D}}} \mathbf{j}_{th}(z) + \int_{\mathcal{D}} \frac{d^d z}{V_{\mathcal{D}}} \mathbf{v}_f(z), \quad (\text{A10})$$

Note that the first term generalizes the result of Ref. [72] to arbitrary dimensions. The second term intuitively states that the condensate is advected by the average flow of the fluid.

Appendix B: Pairwise interactions between condensates

This supporting section presents a generalized scenario in which two condensates labeled $i \in \{1, 2\}$ interact through translation-induced polarization. The domains of these two condensates, \mathcal{D}_i , are centered around $\mathbf{r}_i(t)$, respectively. One premise, which is straightforward to generalize, is that each condensate moves with the same velocity \mathbf{v} when far away from the other condensate. This motion could be induced by phoresis, sedimentation, advection, or optical trapping, but the precise mechanism is of little consequence. More importantly, the motion of each condensate introduces a dipole force field, which will perturb the motion of the other condensate so that $\partial_t \mathbf{r}_i(t) := \mathbf{v} + \delta \mathbf{v}_i$. In the following, the perturbations $\delta \mathbf{v}_i$ will be derived.

According to Eq. (3), the motion of the first condensate gives rise to an additive contribution to the chemical potential profile:

$$\nabla \delta \mu_1(\mathbf{x}, t) = \frac{\Delta c}{M} \mathcal{B}(\mathbf{x} - \mathbf{r}_1 | \mathcal{D}_1) \cdot [\mathbf{v} + \delta \mathbf{v}_1], \quad (\text{B1})$$

where $\mathcal{B}(\mathbf{x} - \mathbf{r}_1 | \mathcal{D}_1)$ is given by Eq. (A3). Using the same notation, we will now discuss the response of the second condensate.

The additional contribution to the chemical potential profile drives a potential flux. Consequently, the second condensate will move according to Eq. (A7):

$$\delta \mathbf{v}_2 = -\frac{d}{\Delta c} \int_{\mathcal{D}_2} \frac{d^d z}{V_{\mathcal{D}_2}} M \nabla \delta \mu_1(\mathbf{r}_2 + \mathbf{z}, t). \quad (\text{B2})$$

Substituting Eq. (B1) in Eq. (B2) and using the definition of the coupling tensor Eq. (A3) leads to

$$\delta \mathbf{v}_2 = \mathbf{M}_{21} \cdot [\mathbf{v} + \delta \mathbf{v}_1], \quad (\text{B3})$$

where the cross-mobility is defined as

$$\mathbf{M}_{21} := \frac{d}{V_{\mathcal{D}_2}} \oint_{\partial \mathcal{D}_2} d\mathbf{S} \otimes \oint_{\partial \mathcal{D}_1} d\mathbf{S}' \mathcal{L}(\mathbf{r}_2 - \mathbf{r}_1 + \mathbf{z} - \mathbf{z}'). \quad (\text{B4})$$

and the integral was simplified using Gauss' theorem. For small condensates that do not overlap, one can make the following approximation:

$$\mathbf{M}_{21} \approx -d V_{\mathcal{D}_1} \nabla \otimes \nabla \mathcal{L}(\mathbf{r}_2 - \mathbf{r}_1). \quad (\text{B5})$$

The response of the first condensate to the motion of the second condensate is analogous, just with flipped indices $1 \leftrightarrow 2$.

To understand under which conditions the two condensates will begin to approach or repel each other, it is useful to track $\partial_t(\mathbf{r}_2 - \mathbf{r}_1)$. Based on the above approximation for small condensate sizes, one can assume that \mathbf{M}_{21} and \mathbf{M}_{12} commute. The separation between the two condensates will then gradually change according to

$$\delta \mathbf{v}_2 - \delta \mathbf{v}_1 \approx [\mathbf{I} - \mathbf{M}_{21} \cdot \mathbf{M}_{12}]^{-1} \cdot (\mathbf{M}_{21} - \mathbf{M}_{12}) \cdot \mathbf{v}. \quad (\text{B6})$$

For large separations between the condensates, the term in square brackets is approximately equal to the identity matrix. Thus, for large separations compared to the condensate size, one can further simplify:

$$\partial_t(\mathbf{r}_2 - \mathbf{r}_1) \approx d (V_{\mathcal{D}_2} - V_{\mathcal{D}_1}) \nabla \otimes \nabla \mathcal{L}(\mathbf{r}_2 - \mathbf{r}_1) \cdot \mathbf{v}, \quad (\text{B7})$$

after substituting the cross-mobility Eq. (B5). For spherical condensates in $d = 3$ dimensions, one has $\mathcal{L}(\mathbf{z}) = 1/(4\pi|\mathbf{z}|)$ and $V_{\mathcal{D}_1} = 4\pi/3 R_1^3$, leading to

$$\partial_t(\mathbf{r}_2 - \mathbf{r}_1) \approx (R_2^3 - R_1^3) \nabla \otimes \nabla \frac{1}{|\mathbf{r}_2 - \mathbf{r}_1|} \cdot \mathbf{v}, \quad (\text{B8})$$

which was reported in the main text.

Appendix C: Response of the fluid flow to condensate motion

This supporting section analyzes how the embedding fluid will respond to the motion of condensates and under which conditions this response can be neglected. The present manuscript focuses on the dynamics of a viscoelastic fluid according to Eq. (13) with Green's function

Eq. (14). In the present section, we will discuss a general linear response theory in which the fluid flow is given by:

$$\mathbf{v}_f(\mathbf{x}, t) = \int d^d \mathbf{x}' \int_{-\infty}^t dt' \mathcal{G}(\mathbf{x} - \mathbf{x}', t - t') \cdot \mathbf{f}(\mathbf{x}', t'), \quad (\text{C1})$$

with driving force $\mathbf{f} := \nabla \cdot \boldsymbol{\alpha} - c \nabla \mu$. The idea is to split the flow into two contributions, $\mathbf{v}_f = \mathbf{v}_f^* + \delta \mathbf{v}_f$, where

$$\mathbf{v}_f^*(\mathbf{x}, t) = \int d^d \mathbf{x}' \int_{-\infty}^t dt' \mathcal{G}(\mathbf{x} - \mathbf{x}', t - t') \cdot \nabla \cdot \boldsymbol{\alpha}(\mathbf{x}', t') \quad (\text{C2})$$

arises from active and passive forces that are independent of the condensates, and

$$\delta \mathbf{v}_f(\mathbf{x}, t) = - \int d^d \mathbf{x}' \int_{-\infty}^t dt' \mathcal{G}(\mathbf{x} - \mathbf{x}', t - t') \cdot c \nabla \mu(\mathbf{x}', t') \quad (\text{C3})$$

models the perturbation of the fluid flow by the condensates. In the following, the latter will be analyzed in detail.

First, after using $c(\mathbf{x}, t) = c_- + \Delta c$ for $\mathbf{x} \in \mathcal{D}(t)$, else c_- , to split the domain integral, one has:

$$\begin{aligned} \delta \mathbf{v}_f(\mathbf{x}, t) = & - \int_{-\infty}^t dt' \left[\right. \\ & + c_- \int d^d \mathbf{x}' \mathcal{G}(\mathbf{x} - \mathbf{x}', t - t') \cdot \nabla \mu(\mathbf{x}', t') \\ & \left. + \Delta c \int_{\mathcal{D}(t')} d^d \mathbf{x}' \mathcal{G}(\mathbf{x} - \mathbf{x}', t - t') \cdot \nabla \mu(\mathbf{x}', t') \right]. \quad (\text{C4}) \end{aligned}$$

The second line can be eliminated via integration by parts, by using fluid incompressibility $\nabla \cdot \mathcal{G} = 0$ and the fact that the Green's function decays to zero in the far field. Hence, the perturbation of the fluid flow is given by

$$\begin{aligned} \delta \mathbf{v}_f(\mathbf{x}, t) = & - \Delta c \int_{-\infty}^t dt' \times \\ & \times \int_{\mathcal{D}(t')} d^d \mathbf{x}' \mathcal{G}(\mathbf{x} - \mathbf{x}', t - t') \cdot \nabla \mu(\mathbf{x}', t'). \quad (\text{C5}) \end{aligned}$$

The next step is to substitute the expression for the gradient of the chemical potential, Eq. (A2), with nonpotential flux $\mathbf{j} := c \mathbf{v}_f$.

As before, Eq. (A2) can be simplified by splitting the domain integral according to $c(\mathbf{x}, t) = c_- + \Delta c$ for $\mathbf{x} \in \mathcal{D}(t)$, else c_- . The term proportional to c_- is eliminated via integration by parts, after replacing $\nabla_{\mathbf{x}} \mathcal{L}(\mathbf{x} - \mathbf{x}') = -\nabla_{\mathbf{x}'} \mathcal{L}(\mathbf{x} - \mathbf{x}')$, by using fluid incompressibility and the fact that \mathcal{L} decays to zero in the far field. Taken together, the chemical potential profile in the laboratory frame is given by:

$$\begin{aligned} \nabla \mu(\mathbf{x}, t) = & -\nabla \Psi(\mathbf{x}, t) + \frac{\Delta c}{M} \mathcal{B}(\mathbf{x} - \mathbf{r}) \cdot \mathbf{v}(t) \\ & - \frac{\Delta c}{M} \int_{\mathcal{D}(t)} d^d \mathbf{x}' [\nabla \otimes \nabla \mathcal{L}(\mathbf{x} - \mathbf{x}')] \cdot \mathbf{v}_f(\mathbf{x}', t), \quad (\text{C6}) \end{aligned}$$

where $\mathbf{r} \equiv \mathbf{r}(t)$. The second term demonstrates how the motion of the condensate, with velocity \mathbf{v} , induces a long-range force on the fluid, with the tensor \mathcal{B} defined by Eq. (A4). Together with Eq. (C5), this result illuminates that the effect of condensate motion on fluid flow is $\mathcal{O}(\Delta c^2)$ and that it decays with the mobility of the phase-separating molecules, $\propto 1/M$. The present manuscript neglects these higher-order corrections to the fluid flow.

Nevertheless, I will briefly comment on how to make such corrections for spherical condensates with radius R , center of mass position $\mathbf{r}(t) \in \mathcal{D}(t)$ and velocity $\mathbf{v} \equiv \mathbf{v}(t)$. This will be illustrated for a single condensate and is straightforward to generalize to a collection of topologically distinct phase-separated domains. In essence, after inserting the chemical potential gradient generated by the condensate, Eq. (C6), into Eq. (C5), one has:

$$\begin{aligned} \delta \mathbf{v}_f(\mathbf{x}, t) = & \frac{\Delta c^2}{M} \int_{-\infty}^t dt' \int_{\mathcal{D}(t')} d^d \mathbf{x}' \left\{ \right. \\ & + \mathcal{G}(\mathbf{x} - \mathbf{x}', t - t') \cdot \left[\frac{\mathbf{v}(t')}{d} + \frac{M \nabla \Psi(\mathbf{x}', t')}{\Delta c} \right] \\ & \left. + \mathcal{G}'(\mathbf{x} - \mathbf{r}', \mathbf{x}' - \mathbf{r}', t - t') \cdot \mathbf{v}_f(\mathbf{x}', t') \right\}, \quad (\text{C7}) \end{aligned}$$

where the time-dependent domain $\mathcal{D}(t')$ of the condensate is centered around $\mathbf{r}' \equiv \mathbf{r}(t')$ and $\mathcal{B}(\mathbf{x}' - \mathbf{r}') = -\mathbf{I}/d$ for $|\mathbf{x}' - \mathbf{r}'| \leq R$. Interestingly, the second line shows that the embedding fluid responds to lowest order as if driven by a point force, although the force generated by condensate motion is nonlocal.

Because $\mathbf{v}_f = \mathbf{v}_f^* + \delta \mathbf{v}_f$, the third line indicates that the disturbance $\delta \mathbf{v}_f$ of the fluid flow must be calculated self-consistently. Here,

$$\mathcal{G}'(\mathbf{x}, \mathbf{x}', t) := \int_{\mathcal{D}} d^d \mathbf{z} \mathcal{G}(\mathbf{x} - \mathbf{z}, t) \cdot \nabla \otimes \nabla \mathcal{L}(\mathbf{z} - \mathbf{x}'), \quad (\text{C8})$$

with \mathcal{D} the time-independent domain of the condensate in the comoving and corotating frame, is a modified Green's function. In future studies, these results can be used to derive an equivalent of the Rotne-Prager-Yamakawa tensor [90, 91] to study fluid-mediated interactions in the context of biomolecular condensates.

Appendix D: Expansion of the fluid flow correlation function

This supporting section details how to characterize the correlation of the fluid flow evaluated at randomly fluctuating locations. To that end, consider a series expansion of the fluid flow field around the midpoint $\bar{\mathbf{r}} := (\mathbf{r} + \mathbf{r}')/2$ of the condensate trajectory in the time window $[t, t']$:

$$\mathbf{v}_f(\mathbf{z} + \mathbf{r}, t) = \sum_n \frac{1}{n!} [(\mathbf{r} - \bar{\mathbf{r}}) \cdot \nabla_{\mathbf{z}}]^n \mathbf{v}_f(\mathbf{z} + \bar{\mathbf{r}}, t), \quad (\text{D1})$$

where $\mathbf{r} \equiv \mathbf{r}(t)$ and $\mathbf{r}' \equiv \mathbf{r}(t')$ are random variables corresponding to the center of mass of the condensate. The covariance of the fluid velocity is then given by:

$$\langle \mathbf{v}_f(\mathbf{z} + \mathbf{r}, t) \cdot \mathbf{v}_f(\mathbf{z}' + \mathbf{r}', t') \rangle = \sum_{nm} \frac{1}{n!m!} \left\langle \left[\frac{\mathbf{r} - \mathbf{r}'}{2} \cdot \nabla_{\mathbf{z}} \right]^n \times \left[\frac{\mathbf{r}' - \mathbf{r}}{2} \cdot \nabla_{\mathbf{z}'} \right]^m \mathbf{v}_f(\mathbf{z} + \bar{\mathbf{r}}, t) \cdot \mathbf{v}_f(\mathbf{z}' + \bar{\mathbf{r}}, t') \right\rangle, \quad (\text{D2})$$

where I have substituted the midpoint of the trajectory. In order to proceed, the idea is to split the correlations of the condensate motion and the correlations of the fluid flow. To that end, I posit that the fluid flow fluctuates much faster than the condensate motion, so that one can make the preaveraging approximation $\mathbf{v}_f(\mathbf{z} + \bar{\mathbf{r}}, t) \cdot \mathbf{v}_f(\mathbf{z}' + \bar{\mathbf{r}}, t') \approx \langle \mathbf{v}_f(\mathbf{z} + \bar{\mathbf{r}}, t) \cdot \mathbf{v}_f(\mathbf{z}' + \bar{\mathbf{r}}, t') \rangle$. Another way to see this is from Eq. (7), which states that the fluid flow is averaged over the condensate size, so that condensate motion is almost independent of the fluid flow through an infinitesimally small region. After substituting the definition of the covariance of the hydrodynamic fluctuations, $\mathcal{C}_f(\mathbf{z} - \mathbf{z}', t - t') := \langle \mathbf{v}_f(\mathbf{z}, t) \cdot \mathbf{v}_f(\mathbf{z}', t') \rangle$, and using $\nabla_{\mathbf{z}'} \mathcal{C}_f(\mathbf{z} - \mathbf{z}', t - t') = -\nabla_{\mathbf{z}} \mathcal{C}_f(\mathbf{z} - \mathbf{z}', t - t')$, one has:

$$\langle \mathbf{v}_f(\mathbf{z} + \mathbf{r}, t) \cdot \mathbf{v}_f(\mathbf{z}' + \mathbf{r}', t') \rangle \approx \sum_{nm} \frac{1}{n!m!} \times \times \left\langle \left[\frac{\mathbf{r} - \mathbf{r}'}{2} \cdot \nabla_{\mathbf{z}} \right]^{n+m} \right\rangle \mathcal{C}_f(\mathbf{z} - \mathbf{z}', t - t'). \quad (\text{D3})$$

The next step in the analysis is to use Wick's theorem:

$$\langle \mathbf{v}_f(\mathbf{z} + \mathbf{r}, t) \cdot \mathbf{v}_f(\mathbf{z}' + \mathbf{r}', t') \rangle \approx \sum_{\substack{nm \\ n+m \text{ even}}} \frac{1}{n!m!} \frac{(n+m)!}{\left(\frac{n+m}{2}\right)!} \times \times \frac{1}{2^{\frac{n+m}{2}}} \left\langle \left[\frac{\mathbf{r} - \mathbf{r}'}{2} \cdot \nabla_{\mathbf{z}} \right]^{\frac{n+m}{2}} \right\rangle \mathcal{C}_f(\mathbf{z} - \mathbf{z}', t - t'). \quad (\text{D4})$$

This expression can be simplified by defining the integer $l = \frac{n+m}{2}$ to reorder the summation and by exploiting isotropy, $\langle \Delta \mathbf{r} \otimes \Delta \mathbf{r} \rangle = \langle |\Delta \mathbf{r}|^2 \rangle \mathbf{I}/d$, leading to:

$$\langle \mathbf{v}_f(\mathbf{z} + \mathbf{r}, t) \cdot \mathbf{v}_f(\mathbf{z}' + \mathbf{r}', t') \rangle \approx \sum_l \sum_{n=0}^{2l} \frac{(2l)!}{n!(2l-n)!} \times \times \frac{1}{l!} \frac{1}{2^l} \left[\frac{1}{4d} \langle [\mathbf{r} - \mathbf{r}']^2 \rangle \nabla_{\mathbf{z}}^2 \right]^l \mathcal{C}_f(\mathbf{z} - \mathbf{z}', t - t'). \quad (\text{D5})$$

Finally, after evaluating the inner sum, one arrives at the equation reported in the main text:

$$\begin{aligned} \langle \mathbf{v}_f(\mathbf{z} + \mathbf{r}, t) \cdot \mathbf{v}_f(\mathbf{z}' + \mathbf{r}', t') \rangle &\approx \sum_l \frac{1}{l!} \left[\frac{1}{2d} \langle [\mathbf{r} - \mathbf{r}']^2 \rangle \nabla_{\mathbf{z}}^2 \right]^l \mathcal{C}_f(\mathbf{z} - \mathbf{z}', t - t') \\ &= \exp \left[\frac{1}{2d} \langle [\mathbf{r} - \mathbf{r}']^2 \rangle \nabla_{\mathbf{z}}^2 \right] \mathcal{C}_f(\mathbf{z} - \mathbf{z}', t - t'). \quad (\text{9}) \end{aligned}$$

Appendix E: Differential equation for mean squared displacement

This supporting section combines the previous results to derive the ordinary differential equation for the mean squared displacement reported in the main text. Moreover, it also illustrates how this ordinary differential equation can be solved numerically. Substituting Eq. (9) into Eq. (8) leads to

$$\begin{aligned} \langle \mathbf{v}(t) \cdot \mathbf{v}(t') \rangle &= D_c \delta(t - t') + \iint_{\mathcal{D}} \frac{d^d \mathbf{z}}{V_{\mathcal{D}}} \frac{d^d \mathbf{z}'}{V_{\mathcal{D}}} \times \\ &\times \exp \left[\frac{1}{2d} \langle [\mathbf{r}(t) - \mathbf{r}(t')]^2 \rangle \nabla_{\mathbf{z}}^2 \right] \mathcal{C}_f(\mathbf{z} - \mathbf{z}', t - t'). \quad (\text{E1}) \end{aligned}$$

Next, after using the identity $\partial_t \partial_{t'} \langle |\mathbf{r}(t) - \mathbf{r}(t')|^2 \rangle = -2 \langle \mathbf{v}(t) \cdot \mathbf{v}(t') \rangle$ and defining the mean squared displacement, $\text{MSD}(t - t') := \langle |\mathbf{r}(t) - \mathbf{r}(t')|^2 \rangle$, one arrives at the following nonlinear differential equation:

$$\begin{aligned} \frac{1}{2} \partial_t^2 \text{MSD}(t) &= D_c \delta(t) + \iint_{\mathcal{D}} \frac{d^d \mathbf{z}}{V_{\mathcal{D}}} \frac{d^d \mathbf{z}'}{V_{\mathcal{D}}} \times \\ &\times \exp \left[\frac{1}{2d} \text{MSD}(t) \nabla_{\mathbf{z}}^2 \right] \mathcal{C}_f(\mathbf{z} - \mathbf{z}', t). \quad (\text{E2}) \end{aligned}$$

This is equivalent to Eq. (10) because the δ -distribution sets an initial condition for the slope of the mean squared displacement, and $\langle \dots \rangle_{\mathcal{D}}$ refers to the spatial averaging over the coordinates \mathbf{z} and \mathbf{z}' inside the phase-separated domain \mathcal{D} .

The subsequent analysis will focus on spherical condensates with radius R . In this case, the differential equation Eq. (E2) can be cast into a numerically more convenient form via a Fourier transform in space and time,

$$\widehat{\mathcal{C}}_f(|\mathbf{q}|, \omega) := \int d^d \mathbf{z} \int dt e^{-i\mathbf{q} \cdot \mathbf{z} - i\omega t} \mathcal{C}_f(\mathbf{z}, t), \quad (\text{E3})$$

$$\mathcal{C}_f(\mathbf{z}, t) := \int \frac{d^d \mathbf{q}}{(2\pi)^d} \int \frac{d\omega}{2\pi} e^{i\mathbf{q} \cdot \mathbf{z} + i\omega t} \widehat{\mathcal{C}}_f(|\mathbf{q}|, \omega), \quad (\text{E4})$$

where I have taken into account the isotropy of the correlation function. This leads to the following equation:

$$\begin{aligned} \frac{1}{2} \partial_t^2 \text{MSD}(t) &= D_c \delta(t) + \frac{d\Gamma(1 + \frac{d}{2})}{\pi^{d/2} R^d} \int \frac{d\omega}{2\pi} e^{i\omega t} \times \\ &\times \int_0^\infty \frac{dq}{q} \exp \left[-\frac{q^2}{2d} \text{MSD}(t) \right] J_{d/2}^2(qR) \widehat{\mathcal{C}}_f(q, \omega), \quad (\text{E5}) \end{aligned}$$

with the form factor given by the Bessel function of the first kind,

$$J_{d/2}(q) = \frac{q^{d/2}}{2^{d/2} \Gamma(1 + \frac{d}{2})} \int_{|\mathbf{x}| \leq 1} \frac{d^d \mathbf{x}}{V_1} e^{i\mathbf{q} \cdot \mathbf{x}}, \quad (\text{E6})$$

where V_1 is the volume of the 1-sphere.

Importantly, if the high-frequency modes of the fluid flow do not decay to zero

$$\widehat{\mathcal{C}}_f(q, \infty) := \lim_{\omega \rightarrow \infty} \widehat{\mathcal{C}}_f(q, \omega) \neq 0, \quad (\text{E7})$$

then this will lead to an additional δ -correlated contribution to the transformed differential equation, Eq. (E5). Hence, I split the correlation function of the fluid flow,

$$\hat{\mathcal{C}}_f(q, \omega) = \hat{\mathcal{C}}_f(q, \infty) + [\hat{\mathcal{C}}_f(q, \omega) - \hat{\mathcal{C}}_f(q, \infty)], \quad (\text{E8})$$

and use the trivial initial condition $\text{MSD}(0) = 0$ to rewrite the differential equation, Eq. (E5):

$$\begin{aligned} \frac{1}{2} \partial_t^2 \text{MSD}(t) &= D_c \delta(t) \\ &+ \frac{d\Gamma(1 + \frac{d}{2})}{\pi^{d/2} R^d} \int_0^\infty \frac{dq}{q} J_{d/2}^2(qR) \hat{\mathcal{C}}_f(q, \infty) \delta(t) \\ &+ \frac{d\Gamma(1 + \frac{d}{2})}{\pi^{d/2} R^d} \int \frac{d\omega}{2\pi} e^{i\omega t} \int_0^\infty \frac{dq}{q} \exp\left[-\frac{q^2}{2d} \text{MSD}(t)\right] \times \\ &\quad \times J_{d/2}^2(qR) [\hat{\mathcal{C}}_f(q, \omega) - \hat{\mathcal{C}}_f(q, \infty)]. \end{aligned} \quad (\text{E9})$$

Note that the mean squared displacement is a symmetric function under time reversal. By integrating Eq. (E9) within an infinitesimally small region around the origin, one can now derive the second initial condition, $\partial_t \text{MSD}(0^+) = D_0$, where

$$D_0 = D_c + \frac{d\Gamma(1 + \frac{d}{2})}{\pi^{d/2} R^d} \int_0^\infty \frac{dq}{q} J_{d/2}^2(qR) \hat{\mathcal{C}}_f(q, \infty). \quad (\text{11})$$

For $t > 0$, where the δ -distributions vanish, one has:

$$\begin{aligned} \frac{1}{2} \partial_t^2 \text{MSD}(t) &= \frac{d\Gamma(1 + \frac{d}{2})}{\pi^{d/2} R^d} \int_0^\infty \frac{dq}{q} \exp\left[-\frac{q^2}{2d} \text{MSD}(t)\right] \times \\ &\quad \times J_{d/2}^2(qR) \int \frac{d\omega}{2\pi} e^{i\omega t} [\hat{\mathcal{C}}_f(q, \omega) - \hat{\mathcal{C}}_f(q, \infty)]. \end{aligned} \quad (\text{E10})$$

Note that since the δ -distributions do not matter for $t > 0$, one can also drop the corresponding terms in Eq. (E10) and Eq. (E2), leading to the expression reported in the main text [Eq. (10)].

Appendix F: Asymptotic limits: short and long time scale dynamics

This supporting section analyzes the asymptotic dynamics of the phase-separated domains on short and long time scales. The dynamics on short time scales is dominated by the initial condition on the slope of the mean squared displacement, $\partial_t \text{MSD}(0^+) = D_0$, with the effective diffusion coefficient given by Eq. (11). Hence, the mean squared displacement grows linearly with time, $\text{MSD}(t) \approx D_0|t|$.

To understand the dynamics on long time scales, it is

useful to integrate Eq. (E5) forward in time:

$$\begin{aligned} \partial_t \text{MSD}(t) &= 2 \int_0^t dt' \left[D_c \delta(t') + \frac{d\Gamma(1 + \frac{d}{2})}{\pi^{d/2} R^d} \int \frac{d\omega}{2\pi} e^{i\omega t'} \times \right. \\ &\quad \times \left. \int_0^\infty \frac{dq}{q} \exp\left[-\frac{q^2}{2d} \text{MSD}(t')\right] J_{d/2}^2(qR) \hat{\mathcal{C}}_f(q, \omega) \right]. \end{aligned} \quad (\text{F1})$$

This expression can be further manipulated by symmetrizing the integration domain, which is enabled by the time-reversal symmetry of the mean squared displacement. Moreover, note that the exponential in the second line has its peak at $t' = 0$ and then monotonically decays. Similar to a saddle-point approximation, one can assume that this decay is dominated by the dynamics on short time scales, where $\text{MSD}(t) \approx D_0|t|$. This approximation breaks down if $\partial_t \text{MSD}(t)$ starts at very small values and then increases dramatically.

Hence, the growth of the mean squared displacement on large time scales is governed by another effective diffusion coefficient:

$$\begin{aligned} D_\infty &\approx D_c + \int_{-\infty}^\infty dt' \frac{d\Gamma(1 + \frac{d}{2})}{\pi^{d/2} R^d} \int \frac{d\omega}{2\pi} e^{i\omega t'} \times \\ &\quad \times \int_0^\infty \frac{dq}{q} \exp\left[-\frac{q^2}{2d} D_0|t'|\right] J_{d/2}^2(qR) \hat{\mathcal{C}}_f(q, \omega), \end{aligned} \quad (\text{F2})$$

where I have defined $D_\infty := \lim_{t \rightarrow \infty} \partial_t \text{MSD}(t)$. Splitting the correlation function of the fluid flow according to Eq. (E8), and performing the Fourier transform, one finds:

$$\begin{aligned} D_\infty &\approx D_0 + \frac{d\Gamma(1 + \frac{d}{2})}{\pi^{d/2} R^d} \int_0^\infty \frac{dq}{q} J_{d/2}^2(qR) \times \\ &\quad \times \int \frac{d\omega}{2\pi} \frac{4dD_0 q^2}{4d^2\omega^2 + D_0^2 q^4} [\hat{\mathcal{C}}_f(q, \omega) - \hat{\mathcal{C}}_f(q, \infty)]. \end{aligned} \quad (\text{12})$$

The second term determines whether condensate motion on large time scales is faster or slower than condensate motion on short time scales.

Appendix G: Parameter estimation

This supporting section reports a simple estimate for the parameter values. For a spherical condensate in $d = 3$ dimensions, the dimensionless ratio

$$\frac{6k_B T}{5\pi\eta R D_c} = \frac{2\Delta\phi^2 R^2}{15a^2}, \quad (\text{G1})$$

determines which term in Eq. (18) is dominant. Here, I have used Stokes' law, $M\nu = 1/(6\pi\eta a)$, for the mobility of a molecule with radius $a \sim 2.5$ nm and molecular volume $\nu = \frac{4\pi}{3} a^3$, and defined the volume fraction difference $\Delta\phi := \Delta c\nu$. Assuming a volume fraction difference

of $\Delta\phi = 0.2$, the second term in Eq. (18) will dominate if the condensate is larger than

$$R \gg \sqrt{\frac{15}{2} \frac{a}{\Delta\phi}} \sim 35 \text{ nm}. \quad (\text{G2})$$

For all practical purposes, this can be considered to always be the case. Otherwise, the condensate size would be on the length scale of the phase-separating molecules.

Appendix H: Numerical calculations

This supporting section details the numerical calculation of the mean squared displacement of spherical condensates with radius R in $d = 3$ dimensions. As discussed in the previous section, the first term in Eq. (18) is negligible for most practical scenarios. Hence, in the following, I make the approximation $D_c \approx 0$. Moreover, for simplicity, I also neglect hydrodynamic screening, $\gamma \approx 0$. With these simplifications, one has

$$D_0 \approx \frac{6k_B T \tau_f^2}{5\pi\eta R \tau_\alpha^2}, \quad (\text{H1})$$

which sets the initial condition $\partial_t \text{MSD}(0^+) = D_0$. The second initial condition, as discussed before, is given by $\text{MSD}(0) = 0$. In the following, I define the ratio between the fluid relaxation time and the stirring time, $\Lambda := \tau_f/\tau_\alpha$, and the Fourier number, $\text{Fo} := \frac{6k_B T \tau_\alpha}{5\pi\eta R^3}$, which relates the stirring time to the characteristic time of diffusive mass transport. For a condensate with radius $R = 100 \text{ nm}$, and a stirring time of $\tau_\alpha = 1 \text{ s}$, the Fourier number is $\text{Fo} \sim 1600$. For a condensate with radius $R = 1 \mu\text{m}$, the Fourier number is $\text{Fo} \sim 1.6$. Finally, I define $s := t/\tau_\alpha$ as the nondimensionalized time and $X(t) := \text{MSD}(t)/R^2$ as the nondimensionalized mean squared displacement.

In summary, the results reported in this manuscript were obtained by solving the following nondimensionalized differential equation:

$$\frac{1}{2} \partial_s^2 X = \frac{15}{4} \text{Fo} [1 - \Lambda^2] e^{-s} K(X), \quad (\text{H2})$$

where

$$K(X) := \int_0^\infty \frac{dq}{q^3} \exp\left[-\frac{q^2}{6} X\right] J_{3/2}^2(q). \quad (\text{H3})$$

The initial condition is

$$\partial_s X(0^+) = \text{Fo} \Lambda^2, \quad (\text{H4})$$

and $X(0) = 0$.

The asymptotic dynamics on short time scales are given by

$$\frac{D_0 \tau_\alpha}{R^2} \approx \text{Fo} \Lambda^2, \quad (\text{H5})$$

and on long time scales are given by

$$\frac{D_\infty \tau_\alpha}{R^2} \approx \text{Fo} \Lambda^2 \left[1 + 45 \frac{1 - \Lambda^2}{\Lambda^2} \int_0^\infty \frac{dq}{q^3} \frac{J_{3/2}^2(q)}{6 + \text{Fo} \Lambda^2 q^2} \right]. \quad (\text{H6})$$

Appendix I: Supporting figures

This supporting section contains a figure that shows the anomalous diffusion of condensates at very high Fourier numbers and, moreover, also considers a scenario at very low Fourier numbers.

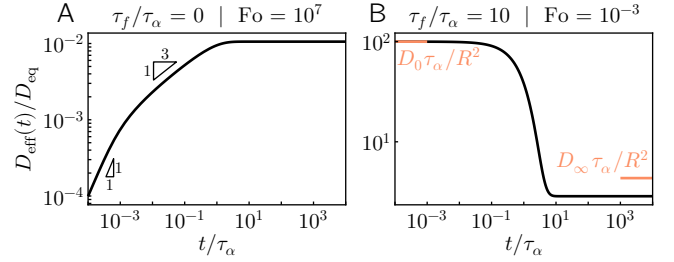


FIG. S1. Effective diffusion coefficient $D_{\text{eff}}(t) := \partial_t \text{MSD}(t)$ of a condensate in a viscoelastic medium compared to Brownian motion $D_{\text{eq}} := 6k_B T/(5\pi\eta R)$ in thermal equilibrium. A) For $\tau_\alpha \gg \tau_f$ and high Fourier numbers, one recovers an intermediate scaling regime indicating superdiffusion with $\text{MSD}(t) \sim t^{4/3}$ as predicted in the main text for viscous fluids in a quenched flow landscape. On short time scales, one finds ballistic motion, whereas on long times one recovers regular diffusion. B) For $\tau_\alpha < \tau_f$ and small Fourier numbers, diffusion on long time scales is much slower than fluctuations on short time scales. Thus, for this parameter regime, there is no superdiffusive transient. In both panels, hydrodynamic screening is assumed to be negligible $\gamma \approx 0$.

[1] M. L. Huggins, Solutions of Long Chain Compounds, *J. Chem. Phys.* **9**, 440 (1941).

[2] P. J. Flory, Thermodynamics of High Polymer Solutions, *J. Chem. Phys.* **9**, 660 (1941).

[3] P. J. Flory, Thermodynamics of High Polymer Solutions, *J. Chem. Phys.* **10**, 51 (1942).

[4] J. W. Cahn and J. E. Hilliard, Free Energy of a Nonuniform System. I. Interfacial Free Energy, *J. Chem. Phys.* **28**, 258 (1958), publisher: American Institute of Physics doi: 10.1063/1.1744102.

[5] J. W. Cahn, On spinodal decomposition, *Acta Metall.* **9**, 795 (1961).

[6] M. Z. Bazant, Theory of Chemical Kinetics and Charge Transfer based on Nonequilibrium Thermodynamics, *Acc. Chem. Res.* **46**, 1144 (2013), doi: 10.1021/ar300145c.

[7] J. Joshi and K. Nandakumar, Computational Modeling of Multiphase Reactors, *Annu. Rev. Chem. Biomol. Eng.* **6**, 1 (2015).

[8] C. P. Brangwynne, C. R. Eckmann, D. S. Courson, A. Rybarska, C. Hoege, J. Gharakhani, F. Jülicher, and A. A. Hyman, Germline P granules are liquid droplets that localize by controlled dissolution/condensation, *Science* **324**, 1729–1732 (2009).

[9] A. A. Hyman, C. A. Weber, and F. Jülicher, Liquid-liquid phase separation in biology, *Annu. Rev. Cell Dev. Biol.* **30**, 39–58 (2014).

[10] S. F. Banani, H. O. Lee, A. A. Hyman, and M. K. Rosen, Biomolecular condensates: organizers of cellular biochemistry, *Nat. Rev. Mol. Cell Biol.* **18**, 285–298 (2017).

[11] A. S. Lyon, W. B. Peebles, and M. K. Rosen, A framework for understanding the functions of biomolecular condensates across scales, *Nat. Rev. Mol. Cell Biol.* **22**, 215–235 (2021).

[12] S. Alberti, A. Gladfelter, and T. Mittag, Considerations and challenges in studying liquid-liquid phase separation and biomolecular condensates, *Cell* **176**, 419–434 (2019).

[13] Y. Shin and C. P. Brangwynne, Liquid phase condensation in cell physiology and disease, *Science* **357**, eaaf4382 (2017).

[14] J.-M. Choi, A. S. Holehouse, and R. V. Pappu, Physical principles underlying the complex biology of intracellular phase transitions, *Annu. Rev. Biophys.* **49**, 1–27 (2020).

[15] D. Hnisz, K. Shrinivas, R. A. Young, A. K. Chakraborty, and P. A. Sharp, A phase separation model for transcriptional control, *Cell* **169**, 13–23 (2017).

[16] B. R. Sabari, A. Dall’Agnese, A. Ann Boija, I. A. Klein, E. L. Coffey, K. Shrinivas, B. J. Abraham, N. M. Hannett, A. V. Zamudio, J. C. Manteiga, C. H. Li, Y. E. Guo, D. S. Day, J. Schuijers, E. Vasile, S. Malik, D. Hnisz, T. I. Lee, I. I. Cisse, R. G. Roeder, P. A. Sharp, A. K. Chakraborty, and R. A. Young, Coactivator condensation at super-enhancers links phase separation and gene control, *Science* **361**, eaar3958 (2018).

[17] K. Shrinivas, B. R. Sabari, E. L. Coffey, I. A. Klein, A. Boija, A. V. Zamudio, J. Schuijers, N. M. Hannett, P. A. Sharp, R. A. Young, and A. K. Chakraborty, Enhancer features that drive formation of transcriptional condensates, *Mol. Cell* **75**, 549 (2019).

[18] J. E. Henninger, O. Oksuz, K. Shrinivas, I. Sagi, G. LeRoy, M. M. Zheng, J. O. Andrews, A. V. Zamudio, C. Lazaris, N. M. Hannett, T. I. Lee, P. A. Sharp, I. I. Cisse, A. K. Chakraborty, and R. A. Young, RNA-mediated feedback control of transcriptional condensates, *Cell* **184**, 207 (2021).

[19] T. Hirose, K. Ninomiya, S. Nakagawa, and T. Yamazaki, A guide to membraneless organelles and their various roles in gene regulation, *Nat. Rev. Mol. Cell Biol.* **24**, 288–304 (2023).

[20] G. P. Faber, S. Nadav-Eliyahu, and Y. Shav-Tal, Nuclear speckles – a driving force in gene expression, *J. Cell Sci.* **135**, jcs259594 (2022).

[21] D. L. J. Lafontaine, J. A. Riback, R. Bascetin, and C. P. Brangwynne, The nucleolus as a multiphase liquid condensate, *Nat. Rev. Mol. Cell Biol.* **22**, 165–182 (2021).

[22] S. F. Banani, A. Goychuk, P. Natarajan, M. M. Zheng, G. Dall’Agnese, J. E. Henninger, M. Kardar, R. A. Young, and A. K. Chakraborty, Active RNA synthesis patterns nuclear condensates, *bioRxiv* [10.1101/2024.10.12.614958](https://doi.org/10.1101/2024.10.12.614958) (2024).

[23] P. W. Voorhees, Ostwald Ripening of Two-Phase Mixtures, *Annu. Rev. Mater. Res.* **22**, 197 (1992).

[24] E. D. Siggia, Late stages of spinodal decomposition in binary mixtures, *Phys. Rev. A* **20**, 595 (1979).

[25] R. Shimizu and H. Tanaka, A novel coarsening mechanism of droplets in immiscible fluid mixtures, *Nat. Commun.* **6**, 7407 (2015), 1509.03385.

[26] J. Happel and H. Brenner, *Low Reynolds number hydrodynamics, with special applications to particulate media*, Mech. Fluids Transp. Process. (1983).

[27] M. Driscoll and B. Delmotte, Leveraging collective effects in externally driven colloidal suspensions: experiments and simulations, *Curr. Opin. Colloid Interface Sci.* **40**, 42 (2019), 1810.12977.

[28] H. Tanaka, Viscoelastic phase separation, *Journal of Physics: Condensed Matter* **12**, R207 (2000).

[29] T. Quail, S. Golfier, M. Elsner, K. Ishihara, V. Murugesan, R. Renger, F. Jülicher, and J. Brugués, Force generation by protein-dna co-condensation, *Nat. Phys.* **17**, 1007–1012 (2021).

[30] A. R. Strom, Y. Kim, H. Zhao, Y.-C. Chang, N. D. Orlovsky, A. Košmrlj, C. Storm, and C. P. Brangwynne, Condensate interfacial forces reposition dna loci and probe chromatin viscoelasticity, *Cell* **187**, 5282 (2024).

[31] T. Wiegand and A. A. Hyman, Drops and fibers — how biomolecular condensates and cytoskeletal filaments influence each other, *Emerg. Top. Life Sci.* **4**, 247–261 (2020).

[32] S. Mohapatra and S. Wegmann, Biomolecular condensation involving the cytoskeleton, *Brain Res. Bull.* **194**, 105–117 (2023).

[33] K. Graham, A. Chandrasekaran, L. Wang, N. Yang, E. M. Lafer, P. Rangamani, and J. C. Stachowiak, Liquid-like condensates mediate competition between actin branching and bundling, *Proc. Natl. Acad. Sci. U.S.A.* **121**, e2309152121 (2024).

[34] R. W. Style, T. Sai, N. Fanelli, M. Ijavi, K. Smith-Mannschott, Q. Xu, L. A. Wilen, and E. R. Dufresne, Liquid-liquid phase separation in an elastic network, *Phys. Rev. X* **8**, 011028 (2018).

[35] K. A. Rosowski, T. Sai, E. Vidal-Henriquez, D. Zwicker, R. W. Style, and E. R. Dufresne, Elastic ripening and inhibition of liquid–liquid phase separation, *Nat. Phys.* **16**, 422–425 (2020).

[36] F. Yuan, H. Alimohamadi, B. Bakka, A. N. Tremontozzi, K. J. Day, N. L. Fawzi, P. Rangamani, and J. C. Stachowiak, Membrane bending by protein phase separation, *Proc. Natl. Acad. Sci. U.S.A.* **118**, e2017435118 (2021).

[37] Y. Qiang, C. Luo, and D. Zwicker, Nonlocal elasticity yields equilibrium patterns in phase separating systems, *Phys. Rev. X* **14**, 021009 (2024).

[38] Q. Yu and A. Košmrlj, Pattern formation of phase-separated lipid domains in bilayer membranes, arXiv 10.48550/arxiv.2309.05160 (2023).

[39] A. Winter, Y. Liu, A. Ziepke, G. Dadunashvili, and E. Frey, Phase separation on deformable membranes: interplay of mechanical coupling and dynamic surface geometry, arXiv 10.48550/arxiv.2409.16049 (2024).

[40] E. Frey and K. Kroy, Brownian motion: a paradigm of soft matter and biological physics, *Annalen der Physik* **14**, 20 (2005).

[41] T. M. Squires and T. G. Mason, Fluid Mechanics of Microrheology, *Annual Review of Fluid Mechanics* **42**, 413 (2010).

[42] D. A. Fletcher and R. D. Mullins, Cell mechanics and the cytoskeleton, *Nature* **463**, 485–492 (2010).

[43] A. Zidovska, D. A. Weitz, and T. J. Mitchison, Micron-scale coherence in interphase chromatin dynamics, *Proc. Natl. Acad. Sci. U.S.A.* **110**, 15555–15560 (2013).

[44] R. Bruinsma, A. Y. Grosberg, Y. Rabin, and A. Zidovska, Chromatin hydrodynamics, *Biophys. J.* **106**, 1871–1881 (2014).

[45] H. A. Shaban, R. Barth, and K. Bystricky, Formation of correlated chromatin domains at nanoscale dynamic resolution during transcription, *Nucleic Acids Res.* **46**, e77–e77 (2018).

[46] C. P. Brangwynne, G. H. Koenderink, F. C. MacKintosh, and D. A. Weitz, Intracellular transport by active diffusion, *Trends Cell Biol.* **19**, 423–427 (2009).

[47] A. Al Jord, G. Letort, S. Chanet, F.-C. Tsai, C. Antoniewski, A. Eichmuller, C. Da Silva, J.-R. Huynh, N. S. Gov, R. Voituriez, M.-E. Terret, and M.-H. Verlhac, Cyttoplasmic forces functionally reorganize nuclear condensates in oocytes, *Nat. Commun.* **13**, 5070 (2022).

[48] G. I. Taylor, The formation of emulsions in definable fields of flow, *Proc. R. Soc. Lond. A* **146**, 501–523 (1934).

[49] H. A. Stone, Dynamics of drop deformation and breakup in viscous fluids, *Annu. Rev. Fluid Mech.* **26**, 65–102 (1994).

[50] F. Caballero and M. C. Marchetti, Activity-suppressed phase separation, *Physical Review Letters* **129**, 268002 (2022).

[51] R. Adkins, I. Kolvin, Z. You, S. Witthaus, M. C. Marchetti, and Z. Dogic, Dynamics of active liquid interfaces, *Science* **377**, 768–772 (2022).

[52] A. Bray, Theory of phase-ordering kinetics, *Advances in Physics* **43**, 357–459 (1994).

[53] C. A. Weber, C. F. Lee, and F. Jülicher, Droplet ripening in concentration gradients, *New J. Phys.* **19**, 053021 (2017).

[54] P. C. Bressloff, Two-dimensional droplet ripening in a concentration gradient, *J. Phys. A* **53**, 365002 (2020).

[55] E. Jambon-Puillet, A. Testa, C. Lorenz, R. W. Style, A. A. Rebane, and E. R. Dufresne, Phase-separated droplets swim to their dissolution, *Nat. Commun.* **15**, 3919 (2024).

[56] V. S. Doan, I. Alshareedah, A. Singh, P. R. Banerjee, and S. Shin, Diffusiophoresis promotes phase separation and transport of biomolecular condensates, *Nat. Commun.* **15**, 7686 (2024).

[57] A. Einstein, Über die von der molekularkinetischen Theorie der Wärme geforderte Bewegung von in ruhenden Flüssigkeiten suspendierten Teilchen, *Ann. Phys.* **322**, 549 (1905).

[58] M. Schmitt and H. Stark, Active Brownian motion of emulsion droplets: Coarsening dynamics at the interface and rotational diffusion, *The European Physical Journal E* **39**, 80 (2016), 1608.02571.

[59] M. E. Cates and E. Tjhung, Theories of binary fluid mixtures: from phase-separation kinetics to active emulsions, *J. Fluid Mech.* **836**, P1 (2018), 1806.01239.

[60] S. Wilken, A. Chaderjian, and O. A. Saleh, Spatial Organization of Phase-Separated DNA Droplets, *Phys. Rev. X* **13**, 031014 (2023).

[61] D. S. W. Lee, C.-H. Choi, D. W. Sanders, L. Beckers, J. A. Riback, C. P. Brangwynne, and N. S. Wingreen, Size distributions of intracellular condensates reflect competition between coalescence and nucleation, *Nat. Phys.* **19**, 586 (2023).

[62] H. Zhang, F. Wang, L. Ratke, and B. Nestler, Brownian motion of droplets induced by thermal noise, *Phys. Rev. E* **109**, 024208 (2024).

[63] R. Balian, *From Microphysics to Macrophysics* (Springer, Berlin, Heidelberg, 2007).

[64] S. R. De Groot and P. Mazur, *Non-Equilibrium Thermodynamics*, Dover Books on Physics (Dover Publications, 2013).

[65] D. Zwicker, The intertwined physics of active chemical reactions and phase separation, *Curr. Opin. Colloid Interface Sci.* **61**, 101606 (2022), 2202.13646.

[66] D. Zwicker, O. W. Paulin, and C. t. Burg, Physics of droplet regulation in biological cells, arXiv 10.48550/arxiv.2501.13639 (2025).

[67] A. Goychuk, L. Demarchi, I. Maryshev, and E. Frey, Self-consistent sharp interface theory of active condensate dynamics, *Phys. Rev. Res.* **6**, 033082 (2024).

[68] J. Romano, R. Golestanian, and B. Mahault, Dynamics of phase-separated interfaces in inhomogenous and driven mixtures (2025), arXiv:2506.19029 [cond-mat.soft].

[69] A. Goychuk, Anomalous diffusion and directed coalescence of condensates in driven media (2025), arXiv:2506.07753 [cond-mat.soft].

[70] E. Hückel and P. Debye, Zur Theorie der Elektrolyte. I. Gefrierpunktserniedrigung und verwandte Erscheinungen, *Phys. Z* **24**, 185 (1923).

[71] A. Kumar and S. A. Safran, Fluctuations and shape dependence of microphase separation in systems with long-range interactions, *Phys. Rev. Lett.* **131**, 258401 (2023).

[72] D. Goh, D. Kannan, P. Natarajan, A. Goychuk, and A. K. Chakraborty, RNA gradients can guide condensates toward promoters: implications for enhancer-promoter contacts and condensate-promoter kissing, *bioRxiv* 10.1101/2024.11.04.621862 (2024).

[73] L. D. Landau and E. M. Lifshitz, *Fluid Mechanics*, second edition ed. (Butterworth-Heinemann, Oxford, 1987).

[74] Y. Baek, A. P. Solon, X. Xu, N. Nikola, and Y. Kafri, Generic long-range interactions between passive bodies

in an active fluid, *Phys. Rev. Lett.* **120**, 058002 (2018).

[75] S. Ro, Y. Kafri, M. Kardar, and J. Tailleur, Disorder-induced long-ranged correlations in scalar active matter, *Phys. Rev. Lett.* **126**, 048003 (2021).

[76] U. S. Schwarz and S. A. Safran, Elastic interactions of cells, *Phys. Rev. Lett.* **88**, 048102 (2002).

[77] S. Bose, P. S. Noerr, A. Gopinathan, A. Gopinath, and K. Dasbiswas, Collective states of active particles with elastic dipolar interactions, *Front. Phys.* **10**, 876126 (2022).

[78] F. Meng, D. Matsunaga, and R. Golestanian, Clustering of magnetic swimmers in a poiseuille flow, *Phys. Rev. Lett.* **120**, 188101 (2018).

[79] Y. I. Li and M. E. Cates, Non-equilibrium phase separation with reactions: a canonical model and its behaviour, *J. Stat. Mech.* **2020**, 053206 (2020).

[80] J. Decayeux, V. Dahirel, M. Jardat, and P. Illien, Spontaneous propulsion of an isotropic colloid in a phase-separating environment, *Physical Review E* **104**, 034602 (2021).

[81] L. Demarchi, A. Goychuk, I. Maryshev, and E. Frey, Enzyme-enriched condensates show self-propulsion, positioning, and coexistence, *Phys. Rev. Lett.* **130**, 128401 (2023).

[82] J. F. Robinson, T. Machon, and T. Speck, Universal limiting behaviour of reaction-diffusion systems with conservation laws, arXiv [10.48550/arxiv.2406.02409](https://arxiv.org/abs/2406.02409) (2024).

[83] P. C. Hohenberg and B. I. Halperin, Theory of dynamic critical phenomena, *Rev. Mod. Phys.* **49**, 435 (1977).

[84] J.-P. Bouchaud and A. Georges, Anomalous diffusion in disordered media: Statistical mechanisms, models and physical applications, *Phys. Rep.* **195**, 127 (1990).

[85] B. Barker, J. B. Bell, and A. L. Garcia, Fluctuating hydrodynamics and the Rayleigh–Plateau instability, *Proc. Natl. Acad. Sci. U.S.A.* **120**, e2306088120 (2023), doi: 10.1073/pnas.2306088120.

[86] J. B. Bell, A. Nonaka, and A. L. Garcia, Comment on “Brownian motion of droplets induced by thermal noise”, *Phys. Rev. E* **111**, 056201 (2025).

[87] H. C. Brinkman, A calculation of the viscous force exerted by a flowing fluid on a dense swarm of particles, *Flow Turbul. Combust.* **1**, 27–34 (1949).

[88] R. W. Zwanzig, Hydrodynamic fluctuations and stokes’ law friction, *J. Res. Natl. Bur. Stand. B*, 143 (1964).

[89] R. Kubo, The fluctuation-dissipation theorem, *Rep. Prog. Phys.* **29**, 255 (1966).

[90] J. Rotne and S. Prager, Variational treatment of hydrodynamic interaction in polymers, *J. Chem. Phys.* **50**, 4831–4837 (1969).

[91] H. Yamakawa, Transport properties of polymer chains in dilute solution: Hydrodynamic interaction, *J. Chem. Phys.* **53**, 436–443 (1970).